subunit (10, 11). Although these originally created forms of mCT did not induce ADP-ribosylation and cAMP formation, they still served as mucosal adjuvants by inducing $CD4^+$ Th2 cells, thereby providing effective help for Ag-specific, mucosal S-IgA, as well as plasma IgG and IgA Ab responses.

It is clearly too dangerous to use an enterotoxin as an adjuvant for mucosal vaccines in humans. Our previous studies have shown that nasally administered nCT accumulates in the olfactory nerves and epithelium (ON/E) and olfactory bulbs (OBs) of mice after binding to GM1 gangliosides (12). Furthermore, nCT as a mucosal adjuvant redirects coadministered protein Ags into these neuronal tissues (12). This finding has provoked some concern about the potential role for ganglioside GM1-binding molecules that target neuronal tissues, including the CNS, in nasal immunization. Although deposition of nCT via the ON/E and OBs did not lead to obvious pathologic changes in brain tissue after nasal administration (13), it has been reported that a human vaccine containing inactivated influenza and nLT as an adjuvant resulted in a very high incidence of Bell's palsy (14, 15). These results strongly indicate that it is essential to develop a safer and more effective nasal adjuvant for human use.

Both nCT and nLT consist of a ring of five B subunits and a single A subunit that is cleaved into A1 and A2 chains. Previous studies showed that the carboxyl terminus of the A2 subunit of nCT contains the ER retention signal tetrapeptide KDEL (RDEL in LT). These results show that the toxin is transported via the vesicles from the plasma membrane to the Golgi compartment with subsequent separation of the A and B subunits of nCT (designated throughout as CT-A and CT-B, respectively). The CT-A subunit is redirected to the plasma membrane by retrograde transport via the ER, whereas the CT-B subunit persists in the Golgi compartment. The intracellular target of toxin is G_s, the stimulatory regulatory component of adenyl cyclase (16, 17). Thus, mutations in KDEL influence the movement of CT from the Golgi apparatus to the ER (18–21). It has previously been shown that mutation in K(R)DEL of both CT and LT delayed the time course of toxin-induced Cl^- secretion. Furthermore, consistent with a slower rate of signal transduction, KDEL mutants trafficked more slowly to the basolateral membrane than did nCT (18, 19).

However, a recent report indicated that mutant LT RDEL retained ADP-ribosyltransferase activity and induced morphological changes in Chinese hamster ovary (CHO) cell cultures (19). In contrast, mCT E112K has proven to be a safe and stable adjuvant (10, 11, 13, 22). The mCT E112K was constructed to be devoid of toxicity while retaining its adjuvant activity. Our previous studies showed that mCT E112K was effective in the murine system. Nasal immunization of OVA, the pneumococcal surface protein A of *Streptococcus pneumoniae*, or diphtheria toxoid plus mCT E112K elicited both Ag-specific IgA and IgG Ab responses in mucosal and systemic immune compartments (10, 11, 13). Although our recent studies showed that mCT E112K did not elicit any neuronal damage based upon nerve growth factor-β1 production in the CNS as well as Ag redirection (23, 24), these studies did not provide any direct information as to whether mCT E112K migrates into the CNS after nasal application. In this regard, we have developed double mutants of CT (dmCTs) by introducing a potent mutation in the ADP-ribosylation activity center and KDEL (E112K/KDEV or E112K/KDGL). Therefore, it is now essential for us to determine whether potentially less trafficking of these new dmCTs, when compared with mCT E112K, will occur in their distribution into the CNS. In this study, we have examined the mucosal adjuvanticity and toxicity of these two dmCTs for our continuing efforts to develop safe and effective nasal adjuvants for mucosal vaccines.

Materials and Methods

Preparation of recombinant mCTs

The plasmids containing nCT or mCT E112K genes were constructed as described previously (10). These plasmids were cloned into pUC119 of a 3.1-kb *EcoRI/PstI* DNA fragment including nCT or mCT E112K genes (10). The KDGL and KDEV mutants were constructed by site-directed mutagenesis in which amino acid substitutions were introduced on a plasmid of nCT using PCR. The following oligonucleotides were used to create genes encoding the mutant toxins KDEV and KDGL: 5′-TAA GGA TGA AGT ATG ATT AAA TTA A-3′ and 5′-TAG AAT TAA GGA TGG ATT ATG ATT A-3′ (mutant codons underlined). To construct dmCT E112K/KDEV and E112K/KDGL, the *BspEI/HincII* fragments including KDEV or KDGL mutations were ligated to a plasmid of mCT E112K. After the DNA sequences were confirmed, pUC119 harboring the mutated CT genes at the *EcoRI/PstI* site were transformed into *E. coli* DH5-α. The *E. coli* strains containing the plasmids for the dmCT genes were grown in Luria-Bertani medium (10 g of NaCl, 10 g of tryptone, and 5 g of yeast extract per liter) with 100 μg/ml ampicillin, and dmCTs were purified according to the method described previously (25). Briefly, the bacteria were harvested and lysed with a sonicator (Insonator 201M; Kubota). The crude lysate was then applied to an immobilized D-galactose column (Pierce) and eluted with galactose. The purified recombinant dmCTs contained <0.05 endotoxin U/μg protein.

Intracellular tracking

Human intestinal epithelial T84 cells were incubated with 10 μg/ml Alexa Fluor 488-conjugated nCT, mCT E112K, dmCT E112K/KDEV, or dmCT E112K/EDGL. To identify their intracellular destination, we used boron dipyrromethane Texas Red ceramide (Invitrogen Life Technologies) as a marker for the Golgi apparatus (26) and ER-Tracker (Invitrogen Life Technologies) Blue-White *p*-xylene-bis-pyridinium bromide as a marker for the ER (27). Boron dipyromethane Texas Red-ceramide was added to individual cultures at a concentration of 5 μM for 10 min before termination of the cultures. Cells were washed once before being further cultured in medium containing 2 μM ER-Tracker for 30 min. After incubation, cells were washed three times with PBS and then fixed with 3.7% formaldehyde in PBS for 10 min at room temperature. After fixation, a Leica TCS SP2-AOBS model confocal microscope or a LMS510 model confocal microscope (Zeiss) was used to visualize the cells. The merged color (yellow) area of each Golgi or ER staining image was picked up using Adobe Photoshop software and converted into a black and white picture. The black area in this black and white picture is based upon the original yellow color and was measured using ImageJ (National Institutes of Health). The condition for picking up the yellow area was saved and applied to all pictures. A monolayer of T84 cells covered most of the dish surface; however, for accuracy, we measured the total pixel area covered with cells in the identical picture using ImageJ software. Thus, each picture covers 12.96 mm^2 of culture surface, which is equal to 262144 pixels. The results were shown as the percentage of yellow color area pixels per the total area pixels covered with cells.

Bioassay and toxicity analysis

We next studied the ability of newly created dmCTs and nCT (List Biological Laboratories) to induce toxic effects on cultured mouse Y-1 adrenal tumor cells, following a previously developed procedure (28). Briefly, serial dilutions of dmCT E112K/KDEV, dmCT E112K/KDGL, mCT E112K, or nCT were added to cultures of Y-1 cells at a density of 5×10^4 cells/well in 0.1 ml of F-10 medium (Invitrogen Life Technologies) containing 15% horse serum and 2.5% FCS and incubated at 37°C with 5% CO_2 for 24 h. Light microscopy was then used to examine cells for morphological changes such as the common "rounding" of cells. The toxin concentration required to initiate the rounding of Y-1 cells was determined. For the cAMP assay, 1.5×10^4 CHO cells in F-10 medium containing 1% FCS were cultured with 100 ng/ml dmCT E112K/KDEV, dmCT E112K/KDGL, mCT E112K, or nCT at 37°C with 5% CO_2 for 18 h. Intracellular cAMP measurement was done with an enzyme immunoassay kit (Amersham Biosciences). The protein amount for some samples was determined with a Coomassie protein assay reagent (Pierce), and the levels of cAMP were expressed as picomoles of cAMP per milligram of protein (10). The mouse ileal loop test was conducted essentially as described previously (29, 30). Briefly, the jejenum was ligated with a piece of cotton thread at a distance of ~3 cm from the pylorus. Immediately after ligation, each loop was injected with 0.1 ml of toxin or PBS (as a control). After 3 h, each loop was hung on a fixed clip and stretched by placing another clip weighing 2 g on the other end of the loop. Then, the length and weight of each loop were

measured. The weight/length ratio (mg/cm) was used to express the intensity of the reaction.

Mice

C57BL/6 mice were obtained from the Frederick Cancer Research Facility (National Cancer Institute, Frederick, MD) as well as Japan SLC at 8–12 wk of age. Upon arrival, all mice were immediately transferred to microisolators, maintained in horizontal laminar flow cabinets, and provided sterile food and water ad libitum. The health of the mice was tested semiannually, and all mice used in experiments were determined to be free of bacterial and viral pathogens.

CNS trafficking

We investigated the distribution of acridinium-labeled toxins in the ON/E and OBs after nasal immunization. In these experiments, we used acridinium-labeled toxins because acridinium is a chemiluminescent molecule that can be triggered with sodium hydroxide and hydrogen peroxide in a luminometer to emit light at 430 nm. Because of its high sensitivity, acridinium can be detected at levels as low as femtograms. nCT, mCT E112K, dmCT E112K/KDEV, and dmCT E112K/KDGL were labeled with acridinium as described elsewhere (31). Five or 0.5 μg of acridinium-labeled nCT, mCT E112K, dmCT E112K/KDEV, or dmCT E112K/KDGL was given nasally, and its distribution in CNS tissues was then checked after 24 h. In some experiments, mice were given nasal OVA plus 0.5 μg of acridinium-labeled nCT, mCT E112K, dmCT E112K/KDEV, or dmCT E112K/KDGL three times at weekly intervals. Seven days after the last immunization, residual amounts of enterotoxin in the CNS tissues were detected. For isolation of CNS tissues, we examined both ON/E and OBs as previously described (12). The levels of acridinium present were determined by triggering with sodium hydroxide and hydrogen peroxide in a luminometer emitting light at 430 nm. The CNS tissues of mice given nasal PBS were examined for their background levels of luminescence. These control values are subtracted from each experimental value.

Nasal immunization and sample collection

C57BL/6 mice were immunized three times at weekly intervals with a nasal dose of 100 μg of OVA (Fraction V; Sigma-Aldrich) and 0.5 μg of nCT, mCT E112K, dmCT E112K/KDEV, or dmCT E112K/KDGL in PBS (11, 22, 32). Plasma and mucosal secretions (nasal washes, saliva, and fecal extracts) were collected on day 21. Saliva was obtained from mice following i.p. injection of 100 μg of sterile pilocarpine hydrochloride (Sigma-Aldrich) (33). Fecal pellets (100 mg) were suspended in 1 ml of PBS containing 0.1% sodium azide and then extracted by vortexing for 5 min. The samples were spun at 10,000 × *g* for 5 min, and the supernatants were collected as fecal extracts (11, 22, 33). The nasal washes were obtained by injecting 1 ml of PBS containing 1% BSA on three occasions into the posterior opening of the nasopharynx with a hypodermic needle (34).

Ab assays

Ab titers in plasma and external secretions were determined by an ELISA (10, 11, 22, 35). Falcon microtest assay plates (BD Biosciences) were coated with an optimal concentration of OVA (100 μl of 1 mg/ml) in PBS overnight at 4°C. Two-fold serial dilutions of samples were added after blocking with PBS containing 1% BSA. To detect Ag-specific Ab levels, HRP-conjugated, goat anti-mouse μ, γ, or α H chain-specific Abs were used (Southern Biotechnology Associates). For IgG Ab subclass determinations, biotinylated mAbs specific for IgG1, IgG2a, IgG2b, and IgG3 (BD Pharmingen) and peroxidase-conjugated goat anti-biotin Ab were used. End point titers were expressed as the last dilution yielding an $OD_{414\ nm}$ of >0.1 U above negative control values after 15 min of incubation.

ELISA for OVA-specific IgE Ab responses

OVA-specific IgE Abs were determined by an ELISA (32). Plasma samples were collected 2 wk after the initial nasal immunization, because our previous studies showed that peak Ag-specific IgE Ab responses were seen at this time point, when mice were immunized with OVA and either nCT or mCT E112K as mucosal adjuvants (11). For detection of OVA-specific plasma IgE Ab levels, 96-well immunoplates (Nunc) were coated with rat anti-mouse IgE mAb (R35-72; BD Pharmingen) and incubated overnight at 4°C. After blocking with 3% BSA in PBS, serial dilutions of plasma samples were added and incubated overnight at 4°C. Following extensive washing, biotinylated OVA was added and the plates were incubated overnight at 4°C. Next, HRP-labeled goat anti-biotin Ab (Vector Laboratories) was added, and the color reaction was developed with 2, 2′-azino-bis(3-ethylbenzthiazoline-6-sulfonic acid) (Sigma). End point titers were expressed as the last dilution yielding an $OD_{414\ nm}$ of >0.1 U above negative control values after 15 min incubation.

Enumeration of Ab-forming cells (AFCs)

The spleen and cervical lymph nodes (CLNs) were removed aseptically, and single-cell suspensions were prepared as described elsewhere (11, 22, 32, 35). The submandibular glands (SMGs) and PBS-perfused lungs were removed aseptically and minced into small fragments. Mononuclear cells were isolated by a combination of an enzymatic dissociation procedure with collagenase type IV (0.5 mg/ml; Sigma-Aldrich) followed by discontinuous Percoll (Amersham Biosciences) gradient centrifugation (33). For isolation of mononuclear cells from NALT and nasal passages (NPs), a modified dissociation method was used based upon a previously described protocol (36–38). Individual NALTs were carefully removed using microsurgical tweezers under a stereoscopic microscope. Following removal of the NALT, the NP tissues were also removed from the nasal cavity. Cells from individual tissues were prepared by gently teasing them through sterile stainless steel screens, followed by enzymatic dissociation using collagenase type IV to obtain single-cell preparations (36–38). Mononuclear cells were purified by discontinuous Percoll gradients (Amersham Biosciences). Mononuclear cells in the interface between the 40 and 75% layers were removed, washed, and resuspended in RPMI 1640 (Mediatech) supplemented with HEPES buffer (15 mM), L-glutamine (2 mM), penicillin (100 U/ml), streptomycin (100 μg/ml), and 10% FCS (complete medium). Cells were then subjected to an OVA-specific ELISPOT assay to detect cells producing IgM, IgG, and IgA AFCs (11, 22, 32, 35). Ninety-six-well nitrocellulose plates (Millipore) were coated with 1 mg/ml OVA for analysis of anti-OVA specific AFCs (11, 32, 33).

OVA-specific T cell responses

$CD4^+$ T cells were purified by the magnetic-activated cell sorter system (Miltenyi Biotec) as described previously (11, 35). Briefly, cells from the spleen and CLNs were incubated in a nylon wool column (Polysciences) to remove B cells and macrophages. Enriched T cell fractions were then incubated with anti-mouse CD4 (GK 1.5) microbeads (Miltenyi Biotec) and passed through a magnetized column. The purified T cell fractions were >97% $CD4^+$ and >99% viable. Cells were resuspended in complete medium, and the purified $CD4^+$ T cells (4×10^6 cells/ml) were cultured with or without 1 mg/ml OVA in the presence of T cell-dependent, mitomycin C-treated splenic APCs. These APCs were derived from naive mice and were placed in 96-well or 24-well tissue culture plates (Corning Glass) for 5 days at 37°C in a moist atmosphere of 5% CO_2 in air. In some experiments, purified $CD4^+$ T cells from CLNs and spleen of naive mice were incubated with anti-CD3 mAb (10 μg/ml)- and anti-CD28 mAb (10 μg/ml)-coated wells for 2 days at 37°C in a moist atmosphere of 5% CO_2 in air.

Proliferation of $CD4^+$ T cells was assessed using a cell proliferation ELISA (Roche Diagnostic Systems). Briefly, 10 μmol of BrdU was added for the final 18 h of incubation. The plates were centrifuged at 300 × *g* for 10 min before drying. The plates were incubated with FixDenat solution (Roche) for 30 min at room temperature. Once the solution had been removed, the cells were labeled with a peroxidase-conjugated anti-BrdU mAb for 90 min at room temperature. The plates were washed with PBS-Tween 20 and then developed using a tetramethyl benzidine substrate solution. Incubations were terminated by addition of 1 M H_2SO_4. The absorbance of samples was measured by an ELISA reader at 450 nm. In some experiments, culture supernatants were harvested after 2 or 5 days of incubation and were then subjected to cytokine-specific ELISA.

Cytokine-specific ELISA

Levels of cytokines in culture supernatants were measured by ELISA. The details of the ELISA for IFN-γ, IL-2, IL-4, IL-5, IL-6, and IL-10 have been described previously (10, 39–41). For coating and detection, the following mAbs were used: for anti-IFN-γ, R4-6A2 and XMG1.2 mAbs; for anti-IL-2, JSE6-1A12 and JES-5H4 mAbs; for anti-IL-4, BVD4-1D11 and BVD6-24G2 mAbs; for anti-IL-5, TRFK-5 and TRFK-4 mAbs; for anti-IL-6, MP5-20F3 and MP5-32C11 mAbs; and for anti-IL-10, JES5-2A5 and JES5-16E3 mAbs. The levels of Ag-specific cytokine production were calculated by subtracting the results of control cultures (e.g., without OVA stimulation) from those of OVA-stimulated T cell cultures. This ELISA was capable of detecting 0.10 ng/ml IFN-γ, 30.5 pg/ml IL-2, 23.4 pg/ml IL-4, 6.1 pg/ml IL-5, 78.1 pg/ml IL-6, and 24.4 ng/ml IL-10.

Statistics

The data are expressed as the mean ± SEM. Each mouse group that received dmCT was compared with the mice given nCT or mCT E112K as

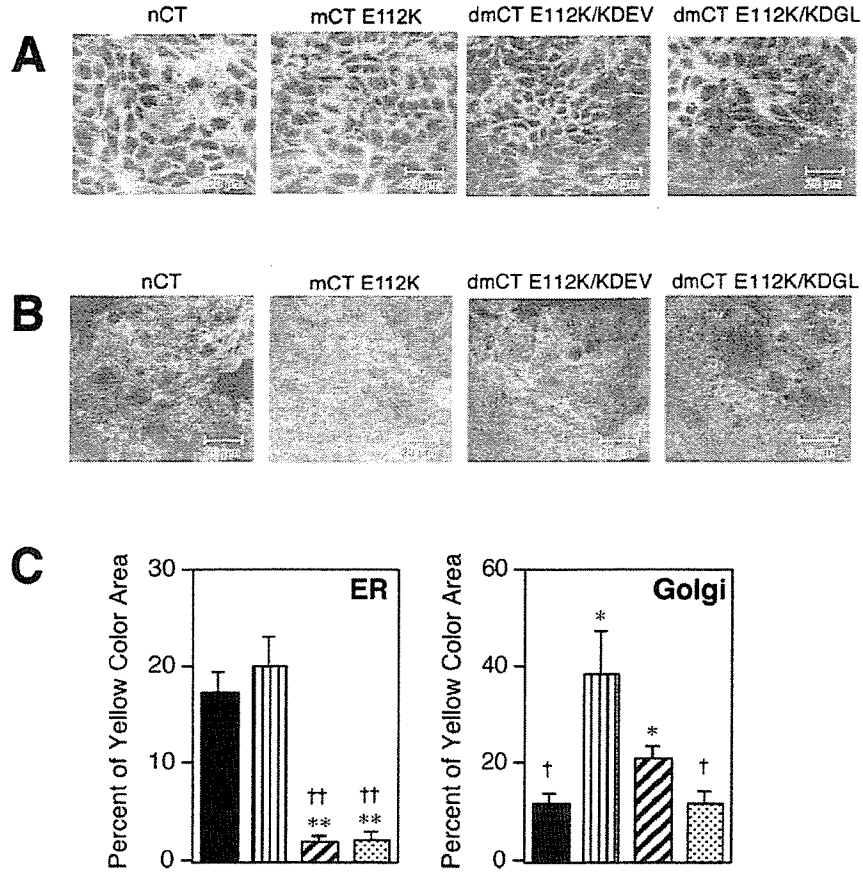

FIGURE 1. Localization of nCT, dmCT E112K/KDEV, dmCT E112K/KDGL, and mCT E112K in T84 cells after incubation. Cells were fixed and analyzed 4 h after the start of Alexa Fluor 488-conjugated nCT, dmCT E112K/KDEV, dmCT E112K/KDGL, and mCT E112K uptake. To identify the intracellular destination, colocalization with ER-Tracker Blue-White *p*-xylene-bis-pyridinium bromide, a marker for the ER, is shown in quasi-red (*A*), whereas BODIPY TR-ceramide, a marker for the Golgi apparatus, is shown in red (*B*). The merged signals appear yellow. Typical image pictures are presented for each group. The yellow color area of nCT (■), mCT E112K (▥), dmCT E112K/KDEV (▨), and dmCT E112K/KDGL (▩) were quantified with ImageJ software (*C*). The values represent the mean ± 1 SEM for six pictures from two different experiments. Each picture covers 12.96 mm^2 of culture surface, which was equal to 262,144 pixels. *, $p < 0.05$; **, $p < 0.01$, when compared with nCT; †, $p < 0.05$; ††, $p < 0.01$, when compared with mCT E112K.

nasal adjuvants using a Mann-Whitney *U* test with StatView II (Abacus Concepts) designed for Macintosh computers. A *p* value of <0.05 or <0.01 was considered significant.

Results

Double mutant CTs fail to track from the Golgi into the ER

Because it has been shown that the COOH terminus of the CT-A subunit KDEL is essential for intracellular movement of CT from the Golgi to the ER, we initially examined intracellular trafficking of our newly developed second generation dmCTs in the T84 human intestinal cell line using confocal microscopic analysis (Fig. 1). After 4 h of incubation, nCT and mCT E112K were detected in the ER of T84 cells (Fig. 1, *A* and *C*, yellow staining); however, dmCT E112K/KDEV and dmCT E112K/KDGL were not detected there (segregated green and red staining; Fig. 1*A*). Thus, the area of yellow staining with both dmCTs was significantly lower than that of nCT and mCT E112K (Fig. 1*C*). Both mCT E112K and dmCT E112K/KDEV were seen in the Golgi apparatus (Fig. 1*B*), and the large area of yellow staining was noted (Fig. 1*C*). Interestingly, the distribution pattern of dmCT E112K/KDEV and dmCT E112K/KDGL differed with the former by being retained longer in the Golgi apparatus than the latter (Fig. 1*B*). Thus, dmCT E112K/KDGL resulted in segregated green and red staining with only a small area of yellow staining (Fig. 1, *B* and *C*). Because a small area of nCT was noted in the Golgi apparatus (Fig. 1*C*), it is

Table I. *Comparison of biologic and toxic activity of mCTs*

Nasal Adjuvant	cAMP Induction[a] (pmol/mg protein)	Y1-Cell Assay[b] (pg/ml)	Ileal Loop Test[c] (W:L ratio)
nCT	104.4 ± 2.3††	0.06 ± 0.01†† (1)[d]	164.3 ± 4.0††
E112K/KDEV	5.3 ± 0.3**	125.0 ± 20.8** (1/2083)	47.7 ± 9.7**
E112K/KDGL	6.5 ± 0.2**	166.7 ± 9.7** (1/2778)	41.7 ± 3.4**
E112K	7.0 ± 1.0**	234.1 ± 44.3* (1/3902)	45.5 ± 0.4**
PBS	7.4 ± 0.5**		37.6 ± 4.4**

[a] CHO cells (1.5×10^4 cells/well) were cultured in F-10 medium containing 1 % FCS with 100 ng/ml of each toxin for 18 h, and the cAMP induction was assessed using an enzyme immunoassay. Values represent the mean ± SEM of nine culture wells in each group. **, $p < 0.01$, when compared with nCT. ††, $p < 0.01$, when compared with mCT E112K.

[b] Y-1 cells were cultured with F-12 medium containing 15% horse serum and 2.5% FCS and serial dilution of each toxin for 24 h. The enterotoxin concentration required to initiate rounding was determined. Values represent the mean ± SEM of of 12 culture wells in each group. *, $p < 0.05$; **, $p < 0.01$, compared with nCT. ††, $p < 0.01$, when compared with mCT E112K.

[c] The ratio of the weight in milligrams to length in centimeters (W:L ratio) after injection of dmCTs into the loop. Each loop was injected with 0.1 ml of 1 μg of dmCTs or nCT. The weight and length of each loop were measured after 3 h values. Values represent the mean ± SEM of six loops in each group. **, $p < 0.01$, when compared with nCT. ††, $p < 0.01$, when compared with mCT E112K.

[d] The values in parenthesis is the ratio of the toxicity of dmCTs to the toxicity of nCT.

Table II. *Comparison of the distribution of dmCTs and nCT in olfactory tissues*

	CNS Tissues					
	ON/E[a]		OBs[a]		ON/E[b]	OBs[b]
Nasal Adjuvants	5 μg	0.5 μg	5 μg	0.5 μg	5 μg	5 μg
nCT	9.61 ± 0.49†[c]	4.03 ± 0.41	1.84 ± 0.55	0.26 ± 0.09	2.23 ± 0.07	1.36 ± 0.02
mCT E112K	3.97 ± 0.37*	4.01 ± 0.65	0.83 ± 0.16	0.12 ± 0.07	1.83 ± 0.19	0.19 ± 0.01**
E112K/KDEV	17.92 ± 1.59*†	4.51 ± 0.58	<0.1**†	<0.1	0.46 ± 0.14**†	<0.1**
E112K/KDGL	14.79 ± 1.07*†	4.73 ± 0.37	0.25 ± 0.03**†	<0.1	0.39 ± 0.01**†	<0.1**

[a] Distribution of acridinium-labeled enterotoxins into the OBs and ON/E was determined 24 h after nasal application of 5 or 0.5 μg of acridinium-labeled nCT, mCT E112K, dmCT E112K/KDEV, or dmCT E112K/KDGL. The OB and ON/E were collected and analyzed for the presence of acridinium-labeled enterotoxin.

[b] Groups of mice were nasally immunized with 100 μg of OVA plus 5 μg of acridinium-labeled nCT, mCT E112K, dmCT E112K/KDEV, or dmCT E112K/KDGL three times at weekly intervals. The distribution of acridinium-labeled enterotoxins in the OBs and ON/E were determined 7 days after the last nasal application. The OBs and ON/E were collected and analyzed for the presence of acridinium-labeled enterotoxin.

[c] Data are expressed as nanograms per 10 mg of tissue ± SEM for nine mice in each experimental group. The CNS tissues of nine mice given nasal PBS were examined for background levels of luminescence. These control values were subtracted from each experimental value. Difference from the value of nCT was statistically significant. (*, $p < 0.05$; **, $p < 0.01$). †, $p < 0.05$, when compared with mCT E112K.

possible that nCT moved quickly into the ER or the surface membrane. In contrast, dmCT E112K/KDGL is most likely redistributed to the surface membrane, because a significantly lower retention signal was found in the ER (Fig. 1*C*). As these results show, because these dmCTs are either retained in the Golgi apparatus (dmCT E112K/KDEV) or redistributed to the surface membrane (dmCT E112K/KDGL), they do not undergo retrograde transport into the ER. In contrast, both nCT and mCT E112K reached the ER within 4 h of incubation.

Enzymatic activity and toxicity of mCTs

The biologic properties and toxicity of dmCTs were examined and compared with those of mCT E112K and nCT (Table I). Essentially no cAMP induction was seen when CHO cells were incubated with dmCTs or mCT E112K. To further examine the toxicity of dmCTs, the morphological changes in Y-1 cells were assessed. Both dmCT E112K/KDEV and E112K/KDGL showed significantly lower toxicity than nCT (1/2083 and 1/2778 of nCT, respectively). In addition, when the mouse ileal loop test was performed to measure toxic manifestations, both dmCTs were found to induce significantly lower levels of fluid accumulation than nCT.

dmCTs do not accumulate in the CNS

To determine whether dmCTs undergo retrograde transport into the CNS, acridinium-labeled dmCT E112K/KDEV, dmCT E112K/KDGL, mCT E112K, or nCT were given by the nasal route. Twenty-four hours after nasal administration of 0.5 μg of nCT, mCT E112K, dmCT E112K/KDEV, and dmCT E112K/KDGL, similar levels of all administered enterotoxins could be detected in the ON/E, but no significant accumulation of the enterotoxins was seen in the OBs (Table II). Accumulation in the ON/E appeared to be dose dependent. Thus, 2- to 4-fold higher quantities of nCT and dmCTs were found in the ON/E after nasal delivery of a 5-μg dose (Table II). At a 5-μg nasal dose, dmCTs accumulated more in the ON/E of mice than did nCT or mCT E112K, but nCT accumulated in the OBs whereas dmCTs did not (Table II). Furthermore, some mCT E112K accumulation was seen in the OBs, although the levels were lower than that of nCT (Table II). The residual levels of dmCT-acridinium compounds in ON/E and OBs were also examined 7 days after the last immunization. Mice were given nasal OVA and acridinium-conjugated nCT, mCT E112K, or dmCTs three times at weekly intervals. Interestingly, no accumulation of either dmCT E112K/KDEV or dmCT E112K/KDGL was detected in the ON/E or the OBs; however, significant amounts of nCT were seen in the OBs (Table II). Furthermore, small amounts of mCT E112K were also detected in the OBs (Table II). Taken together, our studies show that although dmCTs bind and accumulate in the ON/E, these dmCTs do not enter the OBs, whereas nCT quickly traffics into the OBs and remains for at least 7 days after immunization. Furthermore, our findings show that novel dmCTs may have an improved safety profile as nasal adjuvants when compared with mCT E112K, because mCT E112K shows some accumulation in the ON/E and OBs, although the levels were significantly lower than those seen with nCT.

Mucosal adjuvant activity of dmCTs

To assess the mucosal adjuvant properties of dmCTs, the mice were nasally immunized with 100 μg of OVA plus 0.5 μg of dmCT E112K/KDEV, dmCT E112K/KDGL, mCT E112K, or nCT three times at weekly intervals. Plasma and mucosal external secretions (nasal washes, fecal extracts, and saliva) were collected 7 days after the last immunization. Significant levels of OVA-specific S-IgA Ab responses were seen in all external secretions of mice nasally immunized with OVA plus dmCT E112K/KDEV or E112K/KDGL. However, mCT E112K exhibited significantly lower OVA-specific IgA Ab responses in mucosal external secretions than did nCT (Fig. 2). Elevated levels of OVA-specific IgG Ab responses were seen in mice given nasal dmCTs as mucosal adjuvants. OVA-specific IgG Ab responses in mice immunized

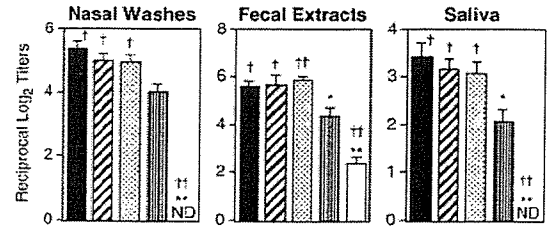

FIGURE 2. Comparison of OVA-specific IgA Ab responses in nasal washes, fecal extracts, and saliva of mice immunized with OVA plus nCT, mCT, or dmCTs. Each mouse group was nasally immunized once a week for three consecutive weeks with 100 μg of OVA plus 0.5 μg of nCT (■), dmCT E112K/KDEV (▨), dmCT E112K/KDGL (▩), mCT E112K (▥), or PBS (□) as mucosal adjuvant. Seven days after the last immunization, the IgA levels in nasal washes and saliva were determined by an OVA-specific ELISA. The values shown are the mean ± 1 SEM for 30 mice in each experimental group. ND indicates that the titer was not detectable. *, $p < 0.05$; **, $p < 0.01$, when compared with nCT; †, $p < 0.05$; ††, $p < 0.01$, when compared with mCT E112K.

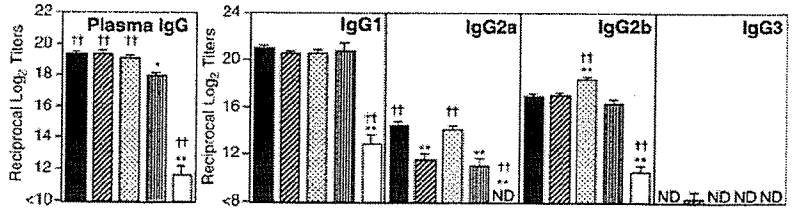

FIGURE 3. Comparison of OVA-specific plasma IgG and IgG subclass Ab responses of C57BL/6 mice nasally immunized with OVA plus nCT, mCT, or dmCTs. Each mouse group was nasally immunized once a week for three consecutive weeks with 100 μg of OVA plus 0.5 μg of nCT (■), dmCT E112K/KDEV (▨), dmCT E112K/KDGL (▤), mCT E112K (▥), or PBS (□) as mucosal adjuvant. Seven days after the last immunization, plasma IgG and IgG subclass Ab levels were determined by OVA-specific ELISA. The values shown are the mean ± 1 SEM for 30 mice in each experimental group. ND, not detected. *, $p < 0.05$; **, $p < 0.01$, when compared with nCT. †, $p < 0.05$; ††, $p < 0.01$, when compared with mCT E112K.

with OVA plus dmCT E112K/KDEV or dmCT E112K/KDGL were identical with those seen in mice given nasal OVA plus nCT (Fig. 3). In contrast, mice given nasal mCT E112K as a mucosal adjuvant showed significant but lower OVA-specific IgG Ab responses than did mice immunized with OVA plus dmCTs or nCT (Fig. 3).

Furthermore, plasma OVA-specific IgG subclass Ab responses were also examined. High levels of OVA-specific-IgG1 and IgG2b Ab responses were seen in mice nasally immunized with OVA plus dmCT E112K/KDEV or E112K/KDGL, as well as in mice given nCT. Although OVA-specific IgG2a Ab responses were relatively lower than those of the IgG1 and IgG2b subclasses, anti-OVA IgG2a titers were significant in mice given nasal nCT or dmCT E112K/KDGL but reduced in those given dmCT E112K/KDEV or mCT E112K. An OVA-specific IgE ELISA revealed elevated levels of OVA-specific IgE Ab responses in plasma of mice given OVA plus nCT (Table III). Most interestingly, significantly lower levels of OVA-specific IgE Abs were noted in mice given nasal OVA plus dmCTs as well as mCT as a nasal adjuvant (Table III).

OVA-specific AFC responses to mCTs

The results of OVA-specific Ab responses were further confirmed at the B cell level by using an OVA-specific ELISPOT assay (Fig. 4). Mononuclear cells from spleens, CLNs, lung, NPs, SMGs, and NALT of mice nasally immunized with OVA plus nCT, mCT E112K, dmCT E112K/KDEV, or dmCT E112K/KDGL were subjected to an OVA-specific ELISPOT assay to determine the numbers and isotypes of AFCs present. In the spleen, CLNs, NPs, and lungs of mice given nasal OVA plus dmCT E112K/KDEV or E112K/KDGL, OVA-specific IgG AFC were elevated to levels comparable to those seen in mice given nCT as nasal adjuvant. In contrast, nasal administration of mCT E112K resulted in levels of anti-OVA IgG AFCs in spleen, CLNs, and lungs that were lower than those seen with dmCTs and nCT. Furthermore, both dmCT E112K/KDEV and dmCT E112K/KDGL induced high numbers of OVA-specific IgA AFCs in NALT, SMGs, and NPs. These results clearly show that the newly developed second generation of dmCT E112K/KDEV and dmCT E112K/KDGL induces Ag-specific Ab responses as effectively as nCT in both systemic and mucosal lymphoid tissues.

Table III. *Comparison of OVA-specific IgE Ab responses induced by nCT, mCT, or dmCTs*

Treatment Group[a]	Ag-Specific IgE[b] (reciprocal $\log_2$ titer)
nCT	7.5 ± 0.3††[c]
E112K/KDEV	3.3 ± 0.4**
E112K/KDGL	3.3 ± 0.3**
E112K	2.3 ± 0.2**
PBS	<2

[a] Each mouse group was nasally immunized once a week for two consecutive weeks with 100 μg of OVA plus 0.5 μg of nCT, mCT E112K/KDEV, mCT E112K/KDGL, mCT E112K, or PBS.

[b] Seven days after the last immunization, OVA-specific IgE levels in plasma were determined by ELISA.

[c] The values shown are the mean ± SEM for 6–8 mice in each experimental group. **, $p < 0.01$, when compared with nCT. ††, $p < 0.01$, when compared with mCT E112K.

OVA-specific CD4$^+$ T cell proliferative and cytokine responses

Because nasal immunization with OVA plus either dmCT E112K/KDEV or dmCT E112K/KDGL induced OVA-specific Ab responses in both systemic and mucosal compartments, it was important to examine the nature of OVA-specific CD4$^+$ Th cell responses. We initially assessed OVA-specific CD4$^+$ T cell proliferative responses in spleen and CLNs of mice nasally immunized with OVA plus dmCTs, nCTs, or mCT E112K. Significantly higher OVA-specific CD4$^+$ T cell proliferative responses were seen in the spleen and CLNs of mice immunized with both dmCT E112K/KDEV and dmCT E112K/KDGL than in mice immunized with mCT E112K (Fig. 5). These OVA-specific CD4$^+$ T cell proliferative responses were comparable to those seen in mice given nCT.

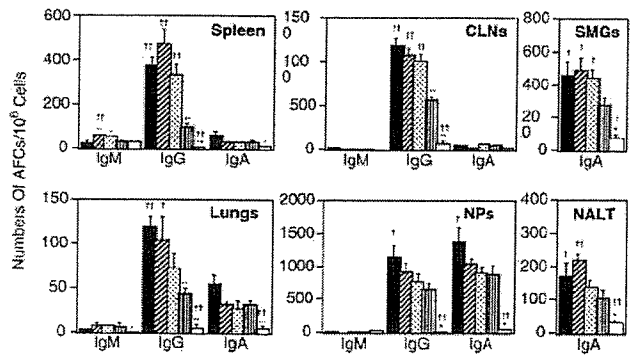

FIGURE 4. Analysis of OVA-specific AFCs in mice immunized nasally with OVA and nCT, mCT, or dmCTs. Each mouse group was nasally immunized once a week for three consecutive weeks with 100 μg of OVA plus 0.5 μg of nCT (■), dmCT E112K/KDEV (▨), dmCT E112K/KDGL (▤), mCT E112K (▥), or PBS (□). Seven days after the last immunization, mononuclear cells isolated from the NPs, SMGs, CLNs, lungs, and spleen were examined using an OVA-specific ELISPOT assay to determine the numbers of IgM, IgG, and IgA AFCs. The results represent the mean values ± 1 SEM for 20 mice in each experimental group. *, $p < 0.05$; **, $p < 0.01$, when compared with nCT. †, $p < 0.05$; ††, $p < 0.01$, when compared with mCT E112K.

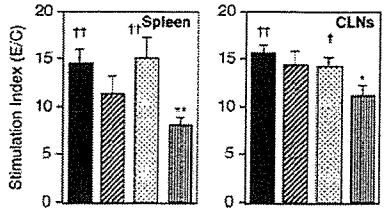

FIGURE 5. Analysis of Ag-specific $CD4^+$ T cell proliferative responses induced by nasal immunization with OVA plus CT derivatives. Each mouse group was nasally immunized once a week for three consecutive weeks with 100 μg of OVA plus 0.5 μg of nCT (■), dmCT E112K/KDEV (▨), dmCT E112K/KDGL (▤), or mCT E112K (▥). The splenic and CLN $CD4^+$ T cells were isolated 7 days after the last immunization and cultured with or without OVA in the presence of APCs. The stimulation index was determined as $A_{450\ nm}$ of wells with OVA divided by wells without OVA (control). The results represent the individual values from three separate experiments. *, $p < 0.05$; **, $p < 0.01$, when compared with nCT; †, $p < 0.05$; ††, $p < 0.01$, when compared with mCT E112K.

We next examined $CD4^+$ Th1- and Th2-type cytokine responses by Ag-specific $CD4^+$ T cells from the spleen and CLNs of mice nasally immunized with OVA plus dmCTs (Fig. 6). Both dmCT E112K/KDEV and dmCT E112K/KDGL induced high levels of Th2-type cytokines (IL-4, IL-5, IL-6, and IL-10) in OVA-stimulated $CD4^+$ T cell cultures. The levels of these cytokines were almost comparable to those seen in OVA-stimulated $CD4^+$ T cells from mice given nCT as nasal adjuvant. Of interest, these Th2-type cytokine responses were comparable to those induced by polyclonal stimulation (solid phase anti-CD3 and anti-CD28 mAb; Fig. 6, dotted lines). In contrast, OVA-stimulated $CD4^+$ T cells from the spleen and CLNs of mice given nasal OVA plus nCT or dmCT E112K/KDGL exhibited similar levels of Th1-type cytokines (IFN-γ and IL-2) (Fig. 6). Although these Th1-type cytokine responses were significantly higher than those responses induced by mCT E112K or dmCT E112K/KDEV as nasal adjuvants, relative Th1-type cytokine production was markedly lower than that induced by anti-CD3 and anti-CD28 mAb stimulation.

Discussion

It is well known that nCT and nLT are effective adjuvants that are capable of enhancing both mucosal S-IgA and systemic IgG Ab responses to coadministered protein Ags in mice and other experimental models. However, both enterotoxins are unsuitable for use in humans due to their toxicity, causing severe diarrhea if given orally and CNS toxicity if administered nasally (14, 15, 42–44). To overcome these obstacles to clinical practicability, several groups, including ours, have focused on developing nontoxic derivatives of CT or LT (10, 16, 17, 45–50). However, although these studies have been successful in producing nontoxic mutants, they did so at times by sacrificing the mucosal adjuvanticity associated with nCT (10, 16, 17, 45–50).

This study shows that a newly developed second generation of dmCTs, which have two amino acid substitutions in the ADP-ribosyltransferase active center (E112K) and COOH-terminal KDEL (dmCT E112K/KDEV or dmCT E112K/KDGL), offer real advantages as nasal adjuvants over the previously developed mCT E112K. When used as nasal adjuvants, even small doses (0.5 μg) of the two dmCTs induced levels of Ag-specific Ab responses in both mucosal and systemic lymphoid tissues that were comparable to those induced by nCT. Unlike nCT, however, that high degree of mucosal adjuvanticity was not accompanied by toxicity. Indeed, both dmCT E112K/KDEV and dmCT E112K/KDGL lacked ADP-ribosyltransferase activity and proved unable to move from the Golgi to the ER. Both dmCTs were thus unable to induce increases in intracellular cAMP. In addition dmCTs did not elicit fluid accumulation in mouse-ligated ileal loops. Furthermore, confocal microscopic analysis showed that the majority of the dmCTs were localized between the surface membranes and the Golgi apparatus

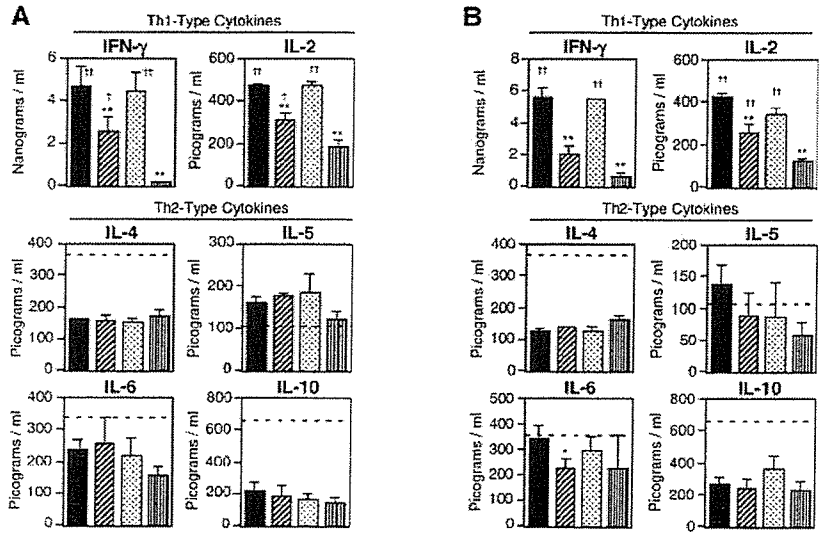

FIGURE 6. OVA-induced $CD4^+$ Th1-type and Th2-type cytokine responses in mice given nasal OVA plus nCT, mCT, or dmCTs. Each mouse group was nasally immunized once a week for three consecutive weeks with 100 μg of OVA plus 0.5 μg of nCT (■), dmCT E112K/KDEV (▨), dmCT E112K/KDGL (▤), or mCT E112K (▥). *A*, The splenic $CD4^+$ T cells (4×10^6 cells/ml) from each mouse group were cultured with 1 mg/ml OVA in the presence of APCs (8×10^6 cells/ml). *B*, The CLN $CD4^+$ T cells (4×10^6 cells/ml) from each mouse group were cultured with 1 mg/ml OVA in the presence of APCs (8×10^6 cells/ml). Culture supernatants were harvested after 5 days of incubation (or after 2 days for IL-2) and analyzed by the respective cytokine-specific ELISA. The dotted lines indicate levels of each cytokine in the wells of anti-CD3 mAb- and anti-CD28 mAb-stimulated $CD4^+$ T cells from spleen or CLNs of naive mice. Th1-type cytokine production by anti-CD3 and anti-CD28 mAb treatments were IFN-γ at ~80 ng/ml and IL-2 at ~10 ng/ml, respectively. The values shown are the mean ± SEM of 15 mice in each group. *, $p < 0.05$; **, $p < 0.01$, when compared with nCT; †, $p < 0.05$; ††, $p < 0.01$, when compared with mCT E112K.

in the T84 cell line and in dendritic cells, and this localization differed from that of mCTs and nCT. Although dmCTs accumulate in the ON/E for a short period, this accumulation did not last and the dmCTs were not transferred into the OBs. Furthermore, nasal application of OVA, together with dmCT E112K/DEV and dmCT E112K/KDGL as adjuvants, resulted in only minimal induction of IgE Ab responses. Collectively, these results indicate that these newly created dmCTs are potent nontoxic mucosal adjuvants suitable for the induction of both mucosal and systemic immune responses in humans.

Although the advantages of nasal immunization have made it the route of choice for the administration of enterotoxins, one area of continuing concern has been the possibility that nasal vaccines could enter the CNS because of the anatomical proximity of the ON/E and OBs to the brain. This potential for neurotoxicity could, of course, rule out the use of enterotoxin-based mucosal adjuvants in humans. Indeed, it was reported that nLT and detoxified LT mutants also targeted the CNS of mice following nasal application (51). In addition, our previous study showed the potential toxicity of CT for the CNS (12). Once CT-B or another nasal enterotoxin vaccine has been associated with neurons via GM1 binding, it cannot be efficiently cleared, and it accumulates in neuronal tissues associated with the olfactory tract tissues (12).

Although our past studies provided evidence that the nCT that accumulates in the olfactory tissue after nasal administration did not lead to obvious pathologic changes in brain tissue (52), our more recent study showed that nasal application of nCT induced nerve growth factor-β, an indicator of nerve cell damage in the olfactory tissues of rhesus macaques (23). We still do not understand the full biological and pathogenic consequences of enterotoxin deposition in the CNS mediated by ganglioside GM1 binding of olfactory tissues; however, it has been shown that a human nasal influenza vaccine with nLT as mucosal adjuvant resulted in the side effect of Bell's palsy (14, 15). It is likely that the nLT was the active component in this vaccine leading to facial paralysis.

In this regard, we have created a second generation of mCTs that avoid transport to the CNS tissues. Our current study clearly shows that dmCTs were not transferred into the OBs, although they were bound and began to accumulate in the ON/E within 24 h. More importantly, the dmCTs that accumulated in the ON/E cleared after 24 h and were not seen in the OBs 7 days after the last immunization even though they were given three times in three consecutive administrations at weekly intervals. Furthermore, because the second generation of dmCTs was designed to avoid cAMP activation by failing to traffic to the ADP-ribosylation activity center, dmCTs did not induce any inflammatory responses despite their early accumulation in the ON/E. Indeed, nasal washes of mice given nasal dmCTs as mucosal adjuvants resulted in essentially no TNF-α production (data not shown). These findings strongly support the safety of newly developed second generation E112K/KDEV and E112K/KDGL dmCTs.

In addition to our current approach, which inhibits intracellular trafficking of the enterotoxin A subunit, others have developed a nCT-based safe and effective adjuvant which targets the Ig receptor on both naive and memory B cells to avoid GM1 ganglioside binding (53). Thus, the enzymatically active A1 subunit of nCT was combined with a dimer of an Ig binding element (DD) from *Staphylococcus aureus* protein A (CT-A1-DD) and coadministered with Ag. This CT-Al-DD adjuvant induced significant Ab and T cell responses without CNS toxicity (53). Furthermore, the same study showed that mCT-A1 E112K-DD failed to elicit adjuvanticity (53). In contrast, others as well as our studies have clearly shown that mCT E112K and dmCTs (E112K/KDEV and E112K/KDGL) retained their nasal adjuvant activities (10, 11, 22, 23). It is possible that the different outcomes between these studies is due to the GM1 ganglioside binding ability of the adjuvants that we have used (10, 13, 17). Thus, mCT and dmCTs target all nucleated cells including professional APCs such as dendritic cells and macrophages, whereas mCT-A1 E112K-DD is limited to binding to B cells. The precise cellular and molecular mechanisms of these new nasal adjuvants needs to be elucidated in future studies. Both dmCTs and CT-A1-DD adjuvants are potential candidates for the development of safe mucosal vaccines.

Past studies have shown that nCT induces marked increases in Ag-specific IgE Ab responses after nasal immunization (10). To develop a mucosal adjuvant that is both safe and effective, the potential for IgE Ab production must be reduced without sacrificing the ability to generate Ag-specific mucosal S-IgA and plasma IgG Ab responses. Our previous studies singled out mCT E112K as the safest and most effective CT-derived adjuvant because it supported Ag-specific S-IgA Ab responses with lower levels of total and anti-CT-B IgE Ab responses than those observed with other enterotoxin-derived adjuvants after nasal immunization (13). Furthermore, when used as a nasal adjuvant, the mCT-A E112K/LT-B chimera, a mCT E112K derivative, induced significantly lower levels of total and Ag-specific IgE Ab responses in the plasma of mice (32). In the current study, we have assessed whether newly created dmCTs induce Ag-specific IgE Ab responses. Our results show that nasal administration of dmCT E112K/KDEV or E112K/KDGL does not enhance IgE Ab responses. Thus, levels of OVA-specific IgE Ab responses were comparable to those elicited by mCT E112K. These results indicate that these dmCT E112K/KDEV and dmCT E112K/KDGL molecules likely avoid allergic reactions to the coadministered Ag and, thus, are promising candidates for being potent nontoxic mucosal adjuvants for human use.

In an attempt to circumvent the toxicity of enterotoxin adjuvants, we developed double mutants of nCT that both lacked the ADP-ribosyltransferase activity and expressed altered ER retention signals (dmCT E112K/KDEV and dmCT E112K/KDGL). To examine the efficacy of these dmCTs for the induction of Ag-specific mucosal S-IgA and systemic IgG Ab responses, we initially used a 5-μg dose of dmCT as nasal adjuvant. We chose this dosage because our previous studies showed that the induction of Ag-specific immune responses in both mucosal and systemic tissues of mice and nonhuman primates required a 10-fold higher dose of mCT E112K/S61F or mCT-A E112K/LT-B than of nCT (2, 10, 11, 23). Because our initial experiments showed dmCTs to be effective adjuvants at the 5-μg dose, we next tested whether 0.5 μg of the newly developed dmCTs could also elicit nasal adjuvanticity. Our results showed both dmCTs to be potent mucosal adjuvants, even when administered at a 10-fold lower rate. In contrast, at a dosage of 0.5 μg, mCT E112K failed to induce the high titers of Ag-specific immune responses seen with nCT.

Although we cannot currently offer a precise explanation for this outcome, it seems clear that the additional point mutation in mCT E112K improves nasal adjuvanticity. Because the structure of the CT molecule is thought to be key to its biological activity (13), there has been concern that the introduction of a point mutation into CT might change or destabilize its own structure and cause diminished mucosal adjuvanticity (13). However, our finding that second generation dmCTs retained nasal adjuvanticity even at lower doses suggests that the molecular structures of dmCTs may be unchanged or stable even after the introduction of double mutations. To explore that possibility, we are currently testing the crystal structures of these dmCTs.

The newly developed dmCTs showed their adjuvant activities through Th2-type cytokine production, especially via an IL-4-dependent mechanism. Thus, nasal immunization with OVA plus dmCT E112K/KDEV or dmCT E112K/KDGL failed to induce OVA-specific Ab responses in IL-4-deficient mice (data not shown). Interestingly, analyses of Th1- and Th2-type cytokine production by $CD4^+$ Th cells revealed that dmCT E112K/KDGL exhibited similar characteristics, especially in the responses of Th1-type cytokine synthesis. Thus, nasal administration of either nCT or dmCT E112K/KDGL resulted in higher levels of IFN-γ and IL-2 production than did that of mCT E112K or dmCT E112K/KDEV, although the levels were relatively lower than the IFN-γ and IL-2 production induced by anti-CD3 and -CD28 mAb treatment. In further support of the similar adjuvant properties shared by nCT and dmCT E112K/KDGL, their OVA-specific plasma IgG2a Ab responses, which are known to be associated with Th1-type cytokines, were significantly higher than those seen in mice given nasal mCT E112K or dmCT E112K/KDEV. We propose that these differences in cytokine profile and OVA-specific IgG subclass Ab responses are due to a difference in the intracellular trafficking of dmCT E112K/KDEV and dmCT E112K/KDGL. These findings indicate that dmCT E112K/KDGL may retain the prototype adjuvanticity of nCT, including the induction of cell-mediated immunity. Because nCT as a nasal adjuvant successfully induced CTL activity by $CD8^+$ T cells, we are currently testing cytokine production and CTL activity by $CD8^+$ T cells from mice given nasal dmCT E112K/KDGL as a mucosal adjuvant.

In summary, a newly developed second generation of both dmCT E112K/KDEV and dmCT E112K/KDGL retained adjuvant activity and elicited mucosal and systemic immunity to nasally coadministered Ags without exhibiting ADP-ribosyltransferase activity or participating in normal intracellular trafficking. Interestingly, like mCT E112K, dmCT E112K/KDEV showed dominant Th2-type cytokine responses. In contrast, like nCT, dmCT E112K/KDGL elicited not only Th2-type cytokine responses but also significantly higher Th1-type cytokine responses than did dmCT E112K/KDEV and mCT E112K. Although different in their immunobiological characteristics, both of our newly developed second-generation dmCTs show promise as effective and safe nasal adjuvants in mice. Future studies will determine whether these adjuvants are safe and effective in both nonhuman primates and humans.

Acknowledgments

We thank Dr. Kimberly K. McGhee for her editorial advice on the manuscript. We also thank Sheila Turner for the final preparation of this manuscript.

Disclosures

The authors have no financial conflict of interest.

References

1. Mestecky, J., R. S. Blumberg, H. Kiyono, and J. R. McGhee. 2003. The mucosal immune system. In *Fundamental Immunology*. W. E. Paul, ed. Lippincott Williams & Wilkins, Philadelphia, p. 965–1020.
2. Hagiwara, Y., J. R. McGhee, K. Fujihashi, R. Kobayashi, N. Yoshino, K. Kataoka, Y. Etani, M. N. Kweon, S. Tamura, T. Kurata, et al. 2003. Protective mucosal immunity in aging is associated with functional $CD4^+$ T cells in nasopharyngeal-associated lymphoreticular tissue. *J. Immunol.* 170: 1754–1762.
3. Holmgren, J., C. Czerkinsky, K. Eriksson, and A. Mharandi. 2003. Mucosal immunisation and adjuvants: a brief overview of recent advances and challenges. *Vaccine* 21: 89–95.
4. Clements, J. D., N. M. Hartzog, and F. L. Lyon. 1988. Adjuvant activity of *Escherichia coli* heat-labile enterotoxin and effect on the induction of oral tolerance in mice to unrelated protein antigens. *Vaccine* 6: 269–277.
5. Katz, J. M., X. Lu, S. A. Young, and J. C. Galphin. 1997. Adjuvant activity of the heat-labile enterotoxin from enterotoxigenic *Escherichia coli* for oral administration of inactivated influenza virus vaccine. *J. Infect. Dis.* 175: 352–363.
6. Elson, C. O., and W. Ealding. 1984. Cholera toxin feeding did not induce oral tolerance in mice and abrogated oral tolerance to an unrelated protein antigen. *J. Immunol.* 133: 2892–2897.
7. Lycke, N., and J. Holmgren. 1986. Strong adjuvant properties of cholera toxin on gut mucosal immune responses to orally presented antigens. *Immunology* 59: 301–308.
8. Marinaro, M., H. F. Staats, T. Hiroi, R. J. Jackson, M. Coste, P. N. Boyaka, N. Okahashi, M. Yamamoto, H. Kiyono, H. Bluethmann, et al. 1995. Mucosal adjuvant effect of cholera toxin in mice results from induction of T helper 2 (Th2) cells and IL-4. *J. Immunol.* 155: 4621–4629.
9. Xu-Amano, J., H. Kiyono, R. J. Jackson, H. F. Staats, K. Fujihashi, P. D. Burrows, C. O. Elson, S. Pillai, and J. R. McGhee. 1993. Helper T cell subsets for immunoglobulin A responses: oral immunization with tetanus toxoid and cholera toxin as adjuvant selectively induces Th2 cells in mucosa associated tissues. *J. Exp. Med.* 178: 1309–1320.
10. Yamamoto, S., Y. Takeda, M. Yamamoto, H. Kurazono, K. Imaoka, M. Yamamoto, K. Fujihashi, M. Noda, H. Kiyono, and J. R. McGhee. 1997. Mutants in the ADP-ribosyltransferase cleft of cholera toxin lack diarrheagenicity but retain adjuvanticity. *J. Exp. Med.* 185: 1203–1210.
11. Yamamoto, S., H. Kiyono, M. Yamamoto, K. Imaoka, K. Fujihashi, F. W. van Ginkel, M. Noda, Y. Takeda, and J. R. McGhee. 1997. A nontoxic mutant of cholera toxin elicits Th2-type responses for enhanced mucosal immunity. *Proc. Natl. Acad. Sci. USA* 94: 5267–5272.
12. van Ginkel, F. W., R. J. Jackson, Y. Yuki, and J. R. McGhee. 2000. Cutting edge: the mucosal adjuvant cholera toxin redirects vaccine proteins into olfactory tissues. *J. Immunol.* 165: 4778–4782.
13. Hagiwara, Y., K. Komase, Z. Chen, K. Matsuo, Y. Suzuki, C. Aizawa, T. Kurata, and S. Tamura. 1999. Mutants of cholera toxin as an effective and safe adjuvant for nasal influenza vaccine. *Vaccine* 17: 2918–2926.
14. Gluck, R., R. Mischler, P. Durrer, E. Furer, A. B. Lang, C. Herzog, and S. J. Cryz, Jr. 2000. Safety and immunogenicity of intranasally administered inactivated trivalent virosome-formulated influenza vaccine containing *Escherichia coli* heat-labile toxin as a mucosal adjuvant. *J. Infect. Dis.* 181: 1129–1132.
15. Durrer, P., U. Gluck, C. Spyr, A. B. Lang, R. Zurbriggen, C. Herzog, and R. Gluck. 2003. Mucosal antibody response induced with a nasal virosome-based influenza vaccine. *Vaccine* 21: 4328–4334.
16. Dickinson, B. L., and J. D. Clements. 1995. Dissociation of *Escherichia coli* heat-labile enterotoxin adjuvanticity from ADP-ribosyltransferase activity. *Infect. Immun.* 63: 1617–1623.
17. Douce, G., C. Turcotte, I. Cropley, M. Roberts, M. Pizza, M. Domenghini, R. Rappuoli, and G. Dougan. 1995. Mutants of *Escherichia coli* heat-labile toxin lacking ADP-ribosyltransferase activity act as nontoxic, mucosal adjuvants. *Proc. Nat. Acad. Sci. USA* 92: 1644–1648.
18. Lencer, W. I., C. Constable, S. Moe, M. G. Jobling, H. M. Webb, S. Ruston, J. L. Madara, T. R. Hirst, and R. K. Holmes. 1995. Targeting of cholera toxin and *Escherichia coli* heat labile toxin in polarized epithelia: role of COOH-terminal KDEL. *J. Cell Biol.* 131: 951–962.
19. Cieplak, W., Jr., R. J. Messer, M. E. Konkel, and C. C. Grant. 1995. Role of a potential endoplasmic reticulum retention sequence (RDEL) and the Golgi complex in the cytotonic activity of *Escherichia coli* heat-labile enterotoxin. *Mol. Microbiol.* 16: 789–800.
20. Majoul, I. V., P. I. Bastiaens, and H. D. Soling. 1996. Transport of an external Lys-Asp-Glu-Leu (KDEL) protein from the plasma membrane to the endoplasmic reticulum: studies with cholera toxin in Vero cells. *J. Cell Biol.* 133: 777–789.
21. Majoul, I., K. Sohn, F. T. Wieland, R. Pepperkok, M. Pizza, J. Hillemann, and H. D. Soling. 1998. KDEL receptor (Erd2p)-mediated retrograde transport of the cholera toxin A subunit from the Golgi involves COPI, p23, and the COOH terminus of Erd2p. *J. Cell Biol.* 143: 601–612.
22. Yamamoto, M., D. E. Briles, S. Yamamoto, M. Ohmura, H. Kiyono, and J. R. McGhee. 1998. A nontoxic adjuvant for mucosal immunity to pneumococcal surface protein A. *J. Immunol.* 161: 4115–4121.
23. Yoshino, N., F. X. Lu, K. Fujihashi, Y. Hagiwara, K. Kataoka, D. Lu, L. Hirst, M. Honda, F. W. van Ginkel, Y. Takeda, et al. 2004. A novel adjuvant for mucosal immunity to HIV-1 gp120 in nonhuman primates. *J. Immunol.* 173: 6850–6857.
24. van Ginkel, F. W., R. J. Jackson, N. Yoshino, Y. Hagiwara, D. J. Metzger, T. D. Connell, H. Lan Vu, M. Martin, K. Fujihashi, and J. R. McGhee. 2005. Enterotoxin-based mucosal adjuvants alter antigen trafficking and induce inflammatory responses in the nasal tract. *Infect. Immun.* 73: 1–11.
25. Uesaka, Y., Y. Otsuka, Z. Lin, S. Yamasaki, J. Yamaoka, H. Kurazono, and Y. Takeda. 1994. Simple method of purification of *Escherichia coli* heat-labile enterotoxin and cholera toxin using immobilized galactose. *Microb. Pathog.* 16: 71–76.
26. Thieblemont, N., and S. D. Wright. 1999. Transport of bacterial lipopolysaccharide to the Golgi apparatus. *J. Exp. Med.* 190: 523–534.
27. Cole, L., D. Davies, G. J. Hyde, and A. E. Ashford. 2000. ER-Tracker dye and BODIPY-brefeldin A differentiate the endoplasmic reticulum and Golgi bodies from the tubular-vacuole system in living hyphae of *Pisolithus tinctorius*. *J. Microsc.* 19: 239–249.
28. Donta, S. T., H. W. Moon, and S. C. Whipp. 1974. Detection of heat-labile *Escherichia coli* enterotoxin with the use of adrenal cells in tissue culture. *Science* 183: 334–336.
29. Yamamoto, K., I. Ohishi, and G. Sakaguchi. 1979. Fluid accumulation in mouse ligated intestine inoculated with *Clostridium perfringens* enterotoxin. *Appl. Environ. Microbiol.* 37: 181–186.

30. Takeda, Y., T. Takeda, T. Yano, K. Yamamoto, and T. Miwatani. 1979. Purification and partial characterization of heat-stable enterotoxin of enterotoxigenic *Escherichia coli*. *Infect. Immun.* 25: 978–985.
31. Miller, S. A., M. S. Morton, and A. Turkes. 1988. Chemiluminescence immunoassay for progesterone in plasma incorporating acridinium ester labelled antigen. *Ann. Clin. Biochem.* 25: 27–34.
32. Kweon, M. N., M. Yamamoto, F. Watanabe, S. Tamura, F. W. Van Ginkel, A. Miyauchi, H. Takagi, Y. Takeda, T. Hamabata, K. Fujihashi, et al. 2002. A nontoxic chimeric enterotoxin adjuvant induces protective immunity in both mucosal and systemic compartments with reduced IgE antibodies. *J. Infect. Dis.* 186: 1261–1269.
33. Fujihashi, K., J. R. McGhee, M. N. Kweon, M. D. Cooper, S. Tonegawa, I. Takahashi, T. Hiroi, J. Mestecky, and H. Kiyono. 1996. γ/δ T cell-deficient mice have impaired mucosal immunoglobulin A responses. *J. Exp. Med.* 183: 1929–1935.
34. Tamura, S., K. Miyata, K. Matsuo, H. Asanuma, H. Takahashi, K. Nakajima, Y. Suzuki, C. Aizawa, and T. Kurata. 1996. Acceleration of influenza virus clearance by Th1 cells in the nasal site of mice immunized intranasally with adjuvant-combined recombinant nucleoprotein. *J. Immunol.* 156: 3892–3900.
35. Koga, T., J. R. McGhee, H. Kato, R. Kato, H. Kiyono, and K. Fujihashi. 2000. Evidence for early aging in the mucosal immune system. *J. Immunol.* 165: 5352–5359.
36. Hiroi, T., K. Iwatani, H. Iijima, S. Kodama, M. Yanagita, and H. Kiyono. 1998. Nasal immune system: distinctive Th0 and Th1/Th2 type environments in murine nasal-associated lymphoid tissues and nasal passage, respectively. *Eur. J. Immunol.* 28: 3346–3353.
37. Asanuma, H., Y. Inaba, C. Aizawa, T. Kurata, and S. Tamura. 1995. Characterization of mouse nasal lymphocytes isolated by enzymatic extraction with collagenase. *J. Immunol. Methods* 187: 41–51.
38. Wu, H. Y., E. B. Nikolova, K. W. Beagley, and M. W. Russell. 1996. Induction of antibody-secreting cells and T-helper and memory cells in murine nasal lymphoid tissue. *Immunology* 88: 493–500.
39. Powers, D. C. 1992. Immunological principles and emerging strategies of vaccination for the elderly. *J. Am. Geriatr. Soc.* 40: 81–94.
40. Schmucker, D. L., M. F. Heyworth, R. L. Owen, and C. K. Daniels. 1996. Impact of aging on gastrointestinal mucosal immunity. *Dig. Dis. Sci.* 41: 1183–1193.
41. Yanagita, M., T. Hiroi, N. Kitagaki, S. Hamada, H. O. Ito, H. Shimauchi, S. Murakami, H. Okada, and H. Kiyono. 1999. Nasopharyngeal-associated lymphoreticular tissue (NALT) immunity: fimbriae-specific Th1 and Th2 cell-regulated IgA responses for the inhibition of bacterial attachment to epithelial cells and subsequent inflammatory cytokine production. *J. Immunol.* 162: 3559–3565.
42. Gorbach, S. L., and C. M. Khurana. 1971. Toxigenic *Escherichia coli* in infantile diarrhea in Chicago. *J. Lab. Clin. Med.* 78: 981–982.
43. Rowe, B., J. Taylor, and K. A. Bettelheim. 1970. An investigation of traveller's diarrhoea. *Lancet* 1: 1–5.
44. Sack, R. B., S. L. Gorbach, J. G. Banwell, B. Jacobs, B. D. Chatterjee, and R. C. Mitra. 1971. Enterotoxigenic *Escherichia coli* isolated from patients with severe cholera-like disease. *J. Infect. Dis.* 123: 378–385.
45. de Haan, L., W. R. Verweij, I. K. Feil, T. H. Lijnema, W. G. Hol, E. Agsteribbe, and J. Wilschut. 1996. Mutants of the *Escherichia coli* heat-labile enterotoxin with reduced ADP-ribosylation activity or no activity retain the immunogenic properties of the native holotoxin. *Infect. Immun.* 64: 5413–5416.
46. Fontana, M. R., R. Manetti, V. Giannelli, C. Magagnoli, A. Marchini, R. Olivieri, M. Domenighini, R. Rappuoli, and M. Pizza. 1995. Construction of nontoxic derivatives of cholera toxin and characterization of the immunological response against the A subunit. *Infect. Immun.* 63: 2356–2360.
47. Giuliani, M. M., G. Del Giudice, V. Giannelli, G. Dougan, G. Douce, R. Rappuoli, and M. Pizza. 1998. Mucosal adjuvanticity and immunogenicity of LTR72, a novel mutant of *Escherichia coli* heat-labile enterotoxin with partial knockout of ADP-ribosyltransferase activity. *J. Exp. Med.* 187: 1123–1132.
48. Lycke, N., T. Tsuji, and J. Holmgren. 1992. The adjuvant effect of *Vibrio cholerae* and *Escherichia coli* heat-labile enterotoxins is linked to their ADP-ribosyltransferase activity. *Eur. J. Immunol.* 22: 2277–2281.
49. Pizza, M., M. R. Fontana, M. M. Giuliani, M. Domenighini, C. Magagnoli, V. Giannelli, D. Nucci, W. Hol, R. Manetti, and R. Rappuoli. 1994. A genetically detoxified derivative of heat-labile *Escherichia coli* enterotoxin induces neutralizing antibodies against the A subunit. *J. Exp. Med.* 180: 2147–2153.
50. Di Tommaso, A., G. Saletti, M. Pizza, R. Rappuoli, G. Dougan, S. Abrignani, G. Douce, and M. T. De Magistris. 1996. Induction of antigen-specific antibodies in vaginal secretions by using a nontoxic mutant of heat-labile enterotoxin as a mucosal adjuvant. *Infect. Immun.* 64: 974–979.
51. Bourguignon, P., V. Henderickx, M. Friede, Y. Lobet, and M. Francotte. 1999. Reactogenicity in the nose and the brain of enterotoxins administered intranasally to mice. In *Molecular Approaches to Vaccine Design, December 2–5.* Cold Spring Harbor Lab. Press, Cold Spring Harbor, NY, p. 23.
52. Hagiwara, Y., T. Iwasaki, H. Asanuma, Y. Sato, T. Sata, C. Aizawa, T. Kurata, and S. Tamura. 2001. Effects of intranasal administration of cholera toxin (or *Escherichia coli* heat-labile enterotoxin) B subunits supplemented with a trace amount of the holotoxin on the brain. *Vaccine* 19: 1652–1660.
53. Eriksson, A. N., Schön, K. M., and Lycke, N. Y. 2004. The cholera toxin-derived CTA1-DD vaccine adjuvant administered intranasally does not cause inflammation or accumulate in the nervous tissues. *J. Immunol.* 173: 3310–3319.

Journal of Medical Microbiology (2006), 55, 1563–1569 DOI 10.1099/jmm.0.46689-0

Genetic characteristics of Matlab variants of *Vibrio cholerae* O1 that are hybrids between classical and El Tor biotypes

Ashrafus Safa,[1] N. A. Bhuyian,[1] Suraia Nusrin,[1] M. Ansaruzzaman,[1] Munirul Alam,[1] T. Hamabata,[2] Yoshifumi Takeda,[3] David A. Sack[1] and G. Balakrish Nair[1]

Correspondence
G. Balakrish Nair
gbnair@icddrb.org

[1]Laboratory Sciences Division, Enteric Microbiology Laboratory, International Centre for Diarrhoeal Disease Research, Bangladesh (ICDDR, B), Centre for Health and Population Research, GPO Box 128, Dhaka 1000, Bangladesh

[2]International Medical Research Center of Japan, Toyama, Tokyo, Japan

[3]Cine-Science Laboratory, Tokiwadai, Tokyo, Japan

The Matlab variants of *Vibrio cholerae* O1, defined as hybrids between the classical and El Tor biotypes, were first isolated from hospitalized patients with acute secretory diarrhoea in Matlab, a rural area of Bangladesh. These variants could not be categorized as classical or El Tor biotypes by phenotypic and genotypic tests, and had representative traits of both the biotypes. A number of virulence-associated genes and/or gene clusters were screened by PCR and DNA sequencing. El Tor-specific gene clusters, *Vibrio* seventh-pandemic islands (VSP)-I and -II and repeat toxin (RTX) were present in the genome of these variants, indicating their El Tor lineage, whereas the nucleotide-sequence-derived CtxB amino acid sequence of these strains grouped them under the classical biotype. Matlab variants possessed all the necessary genes to initiate pandemics. The genetic relatedness of Matlab variants to the *V. cholerae* strains recently isolated in Mozambique is another important observation of this study, which underscores the epidemiological significance of Matlab variants.

Received 20 April 2006
Accepted 18 July 2006

INTRODUCTION

Vibrio cholerae belonging to serogroups O1 and O139 can cause the severe watery diarrhoea known as cholera. To date, more than 200 serogroups of *V. cholerae* have been recognized, based on variable somatic O antigen composition; O1 was the only known epidemic serogroup of *V. cholerae* up to 1991. In 1992, serogroup O139 was recognized as the second epidemic serogroup of *V. cholerae* (Albert *et al.*, 1993; Shimada *et al.*, 1993). There are two well-established biotypes within the *V. cholerae* O1 serogroup, classical and El Tor, which are distinguished from each other by several properties, including haemolysis of sheep red blood cells, agglutination of chicken red blood cells, Voges–Proskauer reaction, and susceptibility to polymyxin B and to biotype-specific phages (Kaper *et al.*, 1995). The first six cholera pandemics are believed to have been caused by the classical biotype, and in 1961, *V. cholerae* strains of El Tor biotype initiated the seventh cholera pandemic, which is still continuing.

Different studies have shown that the virulence of *V. cholerae* O1/O139 involves a number of genes and/or gene clusters. Two large DNA regions, the *Vibrio* pathogenicity island (VPI)-1 and the CTX prophage, encode the major virulence factors in *V. cholerae* O1/O139 (Faruque *et al.*, 1998). The *tcpA* gene of the VPI-1 encodes the major pilin protein which is involved in colonization of *V. cholerae* in the host intestine and also acts as the receptor for CTXΦ to infect *V. cholerae* strains. The core part of the CTXΦ is composed of the genes *psh*, core-encoded pillin (*cep*), $gIII^{CTX}$, *ace* (accessory cholera enterotoxin), *zot* (zonula occludens) and *ctxAB* (Davis & Waldor, 2003). The key virulence factor of *V. cholerae*, cholera toxin (CT), is encoded by the *ctxAB* genes. *cep* is reported to encode a minor coat protein, the function of which is not yet known. Ace and Zot are two CTXΦ-encoded proteins that play a role in phage assembly (Faruque *et al.*, 1998). The $gIII^{CTX}$ gene plays a role in the processes of phage infection and replication (Heilpern & Waldor, 2003). The core part of CTXΦ is usually flanked by a 2·5 kb RS2 region containing

Abbreviations: CCA, chicken red cell agglutination; CT, cholera toxin; MSHA, mannose-sensitive haemagglutinin; RTX, repeat toxin; TLC, toxin-linked cryptic; VPI, *Vibrio* pathogenicity island.

The GenBank/EMBL/DDBJ accession numbers for the *ctxB* gene sequences of *Vibrio cholerae* O1 and O139 are DQ523199–DQ523219.

three ORFs, namely *rstA*, *rstB* and *rstR*, which function in the replication, regulation and integration processes, respectively. In El Tor and O139 strains of toxigenic *V. cholerae* only, CTXΦ is often flanked by an element termed the RS1 element (Waldor *et al.*, 1997; Davis *et al.*, 2000). The RS1 and RS2 regions are similar, except for the *rstC* gene, which is present in the RS1 element alone (Waldor *et al.*, 1997). Mannose-sensitive haemagglutinin (MSHA) is another virulence factor, and encodes a type IV pilus and consists of six ORFs (Jonson *et al.*, 1991; Faruque *et al.*, 1998). Repeat toxin (RTX) is also reported to be virulence-associated, and encodes a protein that has cytotoxic activity (Lin *et al.*, 1999). This cluster comprises four ORFs, *rtxABCD*, of which the *rtxC* gene is seen in the El Tor biotype only. Dziejman *et al.* (2002) have recently reported two other clusters of genes, namely *Vibrio* seventh pandemic island (VSP)-I and -II, which are unique to the *V. cholerae* seventh pandemic El Tor strains. The other genes that may be linked to the pathogenicity of *V. cholerae* include *hlyA*, which encodes a haemolysin that is cytolytic for a variety of erythrocytes and mammalian cells in culture and is rapidly lethal for mice (Kaper *et al.*, 1995); toxin-linked cryptic (TLC), a 4·7 kb DNA fragment whose functional relationship to CTXΦ is not yet understood (Rubin *et al.*, 1998); *pilE*, which encodes a putative fimbrial assembly protein (Heidelberg *et al.*, 2000); and *intI4*, which encodes a previously unknown integrase that recognizes a family of *V. cholerae* repeated sequences (VCRs) associated with a 'gene-VCR' organization, similar to that of the well-characterized antibiotic-resistance integrons (Mazel *et al.*, 1998; Recchia & Hall, 1997).

In our previous studies, we described *V. cholerae* O1 strains that possess both the classical and El Tor attributes and designated these strains as Matlab types I, II and III, as they were first detected in Matlab, a rural area in Bangladesh (Nair *et al.*, 2002). Different phenotypic traits (haemolysis of sheep erythrocytes, agglutination of chicken erythrocytes, sensitivity to polymyxin B and to specific phages, and reaction to the Voges–Proskauer test) and genotypic traits (*ctxA*, *acfB*, *tcpA* and *rstR*) examined in the previous study failed to classify them into classical or El Tor biotypes (Nair *et al.*, 2002). Further characterization of the Matlab type strains by PFGE revealed that type I strains had a classical biotype lineage, whereas types II and III were more closely related to the El Tor biotype (Safa *et al.*, 2005). In this study, we employed extensive PCR-based screening and a DNA-sequence-based approach to examine the different virulence genes and/or gene clusters of Matlab variants and other similar strains, and compared the results with those obtained with reference strains of the classical and El Tor biotypes.

METHODS

Bacterial strains. From the 38 strains of *V. cholerae* O1 and O139 Matlab variants available in our collection, 17 were included in this study. Of these, five *V. cholerae* O1 strains were isolated between 1992 and 1994, and were previously designated Matlab type I (MJ1236, MJ1485), II (MG116226) and III (MG116025, MG116926). The remaining 12 strains (10 *V. cholerae* O1 and two *V. cholerae* O139) were isolated between 1994 and 1997, and have been characterized previously (Nusrin *et al.*, 2004). Three representative strains from previously characterized strains of *V. cholerae* O1 El Tor biotype, isolated in 2004 from Beira, Mozambique, were also included in this study (Ansaruzzaman *et al.*, 2004). All strains were grown in Luria–Bertani (LB) broth and stored as frozen stocks in LB broth with 25 %, v/v, glycerol. *V. cholerae* strain N16961 of El Tor biotype and strain 569B of classical biotype were used as reference strains.

Biotyping. Tests for polymyxin B susceptibility, chicken red cell agglutination (CCA) and phage sensitivity were performed using standard procedures (WHO, 1987).

Genomic DNA isolation and purification. Genomic DNA was extracted and purified from the strains following the method of Sambrook *et al.* (1989), with some modifications. In brief, cells were harvested by centrifugation from overnight-grown cultures in LB and treated with TES (10 mM Tris, pH 8·0, 10 mM EDTA, 100 mM NaCl) and 10 % SDS at 65 °C for 10–15 min. After proteinase K treatment at 50 °C for 18 h, DNA was extracted with phenol/chloroform–isoamyl alcohol (25:24:1) and purified by ethanol precipitation, and dried before dissolving in TE buffer (10 mM Tris/HCl, 1 mM EDTA, pH 8·0). RNase treatment was performed at 37 °C for 1–2 h, and final purification was done by ethanol precipitation. The purified DNA was dissolved in TE buffer and stored at −20 °C, and used for PCR analysis. The purity of the DNA was assayed with a spectrophotometer (GeneQuant) by using automatic calculation of the ratio of A_{260} to A_{280}.

PCR analysis. PCR was used to assay for 11 virulence-associated genes and/or gene clusters in the genome of the 20 *V. cholerae* isolates using 31 sets of PCR primers and conditions described previously (Chow *et al.*, 2001; O'Shea *et al.*, 2004; Rivera *et al.*, 2001). Further, using PRIMER3 software (available at http://www.genome.wi.mit.edu/genome_software/other/primer3.html), six sets of primers were designed (Table 2) to amplify regions that are uniquely present in all El Tor strains but absent in classical strains (Dziejman *et al.*, 2002). PCR was performed in a 25 µl reaction mixture as follows: an initial denaturation step at 96 °C for 5 min, followed by 30 cycles of denaturation at 94 °C for 1 min, primer annealing at 55 °C for 1 min, 1 min of primer extension at 72 °C and 7 min of final extension at 72 °C for one cycle. Amplicons were separated by agarose gel electrophoresis (1 %) in 0·5 × Tris/borate/EDTA buffer. Products were stained with ethidium bromide, destained with distilled water, and visualized under UV light and photographed on a gel-documentation system.

PCR amplification and nucleotide sequencing of *ctxB*. PCR amplification of the *ctxB* gene was performed in a 25 µl reaction mixture in an automated Peltier thermal cycler (PTC-200, MJ Research). PCR primers and conditions were as previously described (Mitra *et al.*, 2000). PCR products were purified with a Microcon centrifugal filter device (Millipore) according to the manufacturer's instructions, and a cycle sequencing reaction was performed in a 20 µl reaction mixture containing 40 ng purified PCR product, 4 µl ready reaction mixture and 3·2 pmol primer. After 25 cycles of amplification, unincorporated nucleotides were removed from the reaction mixture by ethanol precipitation. Dried products were then resuspended in template suppression reagent (TSR) and sequenced based on the dideoxynucleotide chain-termination method with an ABI PRISM BigDye Terminator Cycle Sequencing Reaction kit (Perkin-Elmer Applied Biosystems) on an ABI PRISM 310 automated sequencer.

DNA and protein sequence analysis. The chromatogram sequencing files were inspected using Chromas 2.23 (Technelysium). Nucleotide sequences of the test isolates were compared with the corresponding sequences of the N16961 El Tor reference strain (NC_002505), the 569B classical reference strain (U25679), the O139 reference strain (X76391), and the B33 (AY648939) and B65 (AY648940) strains, retrieved from GenBank using Basic Local Alignment Search Tool (BLAST) (Altschul *et al.*, 1997). Multiple sequence alignments were developed using CLUSTALX 1.81.13, and DNA sequences were translated using GeneDoc version 2.6.002 alignment editor.

RESULTS

All strains tested were resistant to polymyxin B and positive for CCA. Phage typing of seven of the 10 *V. cholerae* O1 strains tested showed resistance to phage IV and susceptibility to phage 5. The remaining strains were resistant to both phages (Table 1). We examined for the presence of the three important virulence-associated genes, namely *tcpA*, *toxT* and *acfB*, of the VPI-1 cluster. Fifteen strains, including three previously characterized strains from Mozambique, showed the presence of *tcpA* of El Tor type, and the remaining five Matlab reference strains (MT-I, MT-II and MT-III) showed *tcpA* of the classical type (Table 1). The remaining two genes were positive for all strains. All strains, including the reference strains, were positive for *rstA*, $gIII^{CTX}$ and *zot* located in the CTX prophage region. Seven strains, including the El Tor N16961 reference strain, were positive for the *rstC* gene, indicating the presence of the RS1 element, while the remaining strains, including the classical reference strain 569B, were negative for *rstC* (Table 1). PCR analysis of all strains tested showed the presence of the MSHA gene cluster. All test strains, including El Tor N16961, showed a positive amplification for the *rtxC* gene of the RTX gene cluster, whereas only classical 569B reference strain was negative for the same gene. Another gene in this cluster, *rtxA*, was present in all the test strains, including classical and El Tor reference strains. Genes in the VSP-I and -II gene clusters were present in all the strains, including the El Tor reference strain, but were absent from the classical reference strain. Four pairs of primers were used to examine four individual loci, namely *hlyA*, *pilE*, *tlc* and *intl4*. Of these, *pilE* and *intl4* were present in all strains tested, including the classical and El Tor reference strains, *hlyA* was present in all except two strains, whereas *tlc* was absent in all strains that were negative for *rstC* (Table 1). PCR analysis of all the six loci that are unique to El Tor strains but absent in classical strains showed the expected size of PCR product in all Matlab type reference strains (MT-I, MT-II and MT-III), including the El Tor reference strain (Fig. 1), but none in the classical reference strain. The deduced amino acid sequence of the CtxB subunit of the single representative strain of Matlab type II and one of two Matlab type III representative strains showed 100 % homology to the N16961 El Tor reference strain of genotype 3, which has tyrosine at position 39, phenylalanine at position 46 and isoleucine at position 68 (Table 1). In contrast, the amino acid sequence of the CT-B subunit of the remaining 12 strains, including two O139 strains, was identical to that of the 569B classical reference strain of genotype 1 (histidine at position 39, phenylalanine at position 46 and threonine at position 68) (Table 1).

DISCUSSION

Molecular studies have shown that the two biotypes of *V. cholerae* O1 originated from separate lineages (Kaper *et al.*, 1982; Karalois *et al.*, 1995). Over time, some of the biotype-specific phenotypic traits have shown variable reactions, as seen in the 1960 pandemic El Tor isolates of *V. cholerae*, which lyse sheep or goat erythrocytes, whereas classical strains are non-haemolytic. The haemolytic trait is now of limited value in differentiating biotypes, since El Tor strains isolated in later years are mostly non-haemolytic (Barrett & Blake, 1981). However, in 1994, El Tor strains from the Gulf Coast of the USA were reported to be strongly haemolytic (Kaper *et al.*, 1995). In our previous study, biotyping of *V. cholerae* O1 strains isolated in Matlab showed variable reactions and therefore we were unable to biotype these strains. We therefore resorted here to genetic screening of different virulence markers in order to understand better the genetic organization of Matlab variants.

The VPI-1 is a large DNA region that is composed of two gene clusters, namely toxin-coregulated pilus (TCP) and accessory colonization factor (ACF) (Herrington *et al.*, 1988; Kovach *et al.*, 1996). The *tcpA* gene of the TCP cluster has alleles specific for classical and El Tor biotypes of O1. In this study, the *tcpA* gene analysis showed variable results, and either a single allele or both the alleles were found among the strains tested (Table 1). Another important gene of this cluster is *toxT*, which encodes a second positive regulatory protein that directly activates a number of virulence genes (DiRita *et al.*, 1996). This gene was present in all the strains tested and indicated the presence of an active virulence-gene regulatory system. Immediately adjacent to and downstream of the TCP cluster the ACF gene cluster is located. This cluster comprises four ORFs (ABCD), and the presence of *acfB*, which encodes a potential colonization factor, in all the strains is significant from the viewpoint of virulence potential. The genes of the MSHA cluster are expressed by strains of the El Tor biotype, but are only rarely expressed by strains of the classical biotype (Jonson *et al.*, 1991). However, all strains in this study were positive for the MSHA gene cluster, including the classical reference strain. The *hlyA* gene is reported to be present in all classical, El Tor and non-O1 strains of *V. cholerae* (Brown & Manning, 1985). In this study, two strains were negative by PCR for this gene, and a further examination can indicate whether the gene is deleted or is present in a mutated form in these two strains. The presence of all these genes, including *pilE* and *intl4*, further indicated the pathogenic potential of these strains.

CT genes were previously identified in all strains examined here (Ansaruzzaman *et al.*, 2004; Nair *et al.*, 2002; Nusrin

Table 1. Phenotypic and genotypic traits of *V. cholerae* O1 and O139 strains

Abbreviations: R, resistant; S, sensitive; C, classical; E, El Tor; Cal, Calcutta type; Env, environmental type; +, positive; −, negative.

Strains	Geographic origin	Year of isolation	Sero-group	Phenotype				Sequence type	Genotype*							
				Polymyxin B	CCA	Phage IV	Phage 5	CtxB subunit sequence	VSP-I (VCO175 VCO180)	Hly (VCO489)	VSP-II (VCO490 VCO517)	VPI-1 (*tcpA*)	RTX (*rtxC*)	RS1 (*rstC*)	CTX (*rstR*†)	TLC (*tlc*)
MJ1236 (MT-I)‡	Bangladesh	1994	O1	R	−	R	R	39 (H), 68 (T)	+	+	+	C	+	−	C	−
MJ1485 (MT-I)‡	Bangladesh	1994	O1	R	−	R	R	39 (H), 68 (T)	+	+	+	C	+	−	C	−
MG116226 (MT-II)‡	Bangladesh	1991	O1	S	−	R	S	39 (Y), 68 (I)	+	+	+	C	+	+	E	+
MG116025 (MT-III)‡	Bangladesh	1991	O1	R	−	R	S	39 (Y), 68 (I)	+	+	+	C	+	+	E	+
MG116926 (MT-III)‡	Bangladesh	1991	O1	R	−	R	S	39 (H), 68 (T)	+	−	+	C	+	+	C, E	+
ML3090	Bangladesh	1996	O1	R	+	R	S	39 (H), 68 (T)	+	−	+	E	+	−	C	−
MJ206	Bangladesh	1994	O1	R	+	R	R	39 (H), 68 (T)	+	+	+	E	+	−	C	−
MJ4298	Bangladesh	1994	O1	R	+	R	S	39 (H), 68 (T)	+	+	+	E	+	−	C	−
MJ5002	Bangladesh	1994	O1	R	+	R	S	39 (H), 68 (T)	+	+	+	E	+	−	C	−
MJ5340	Bangladesh	1994	O1	R	+	R	S	39 (H), 68 (T)	+	+	+	E	+	−	C	−
MJ2894	Bangladesh	1994	O1	R	+	R	R	39 (H), 68 (T)	+	+	+	E	+	−	C	−
MJ591	Bangladesh	1994	O1	R	+	R	R	39 (H), 68 (T)	+	+	+	E	+	−	C	−
MJ382	Bangladesh	1994	O1	R	+	R	S	39 (H), 68 (T)	+	+	+	E	+	−	C	−
MJ1347	Bangladesh	1994	O1	R	+	R	S	39 (H), 68 (T)	+	+	+	E	+	+	C, E	+
MP2071	Bangladesh	1997	O1	R	+	R	S	39 (H), 68 (T)	+	+	+	E	+	+	E, Env	+
MP1950	Bangladesh	2000	O139	R	+	S	S	39 (H), 68 (T)	+	+	+	E	+	+	C, E, Cal	+
MP2044	Bangladesh	2000	O139	R	+	S	S	39 (H), 68 (T)	+	+	+	E	+	+	C, Cal	+
B33‡	Mozambique	2004	O1	R	+	R	S	39 (H), 68 (T)	+	+	+	E	+	−	C	−
B64‡	Mozambique	2004	O1	R	+	R	S	39 (H), 68 (T)	+	+	+	E	+	−	C	−
B180‡	Mozambique	2004	O1	R	+	R	S	39 (H), 68 (T)	+	+	+	E	+	−	C	−
Classical 569B	India	1948	O1	S	−	S	R	39 (H), 68 (T)	−	+	−	C	−	−	C	+
El Tor N16961	Bangladesh	1971	O1	R	+	R	S	39 (Y), 68 (I)	+	+	+	E	+	+	E	+

*Other genes and/or gene clusters, namely MSHA, VPI-1, RTX, *rstA*, *gIII*^{CTX}, *zot*, *ctxAB* and *intI4* were also tested in this study and were positive for all strains.

†*rstR* results have been previously published in Ansaruzzaman *et al.* (2004); Nair *et al.* (2002); Nusrin *et al.* (2004).

‡Polymyxin B, CCA, phage IV and phage 5 results for these strains have been previously published in Ansaruzzaman *et al.* (2004); Nair *et al.* (2002); Nusrin *et al.* (2004).

Table 2. Oligonucleotide primer sequences used in PCR assays for six genetic loci present only in El Tor strains of *V. cholerae*

Annotation no.	Primer sequence	No. of bases	Product size (bp)	Function (Dziejman *et al.*, 2002)
VC1449F	CAGAAATCCAGCAGCAACAA	21	266	Hypothetical protein
VC1449R	TGGGGAAATTTATGATGGAGA	20		
VCA0316F	TCATGCTGATAGCCTGCATT	20	335	Putative acetyl transferase
VCA0316R	TATGCCTATCCCCAATCTCG	20		
VCA0417F	CCAAGCTCTCGGAATCCATA	20	249	Putative acetyl transferase
VCA0417R	CTATCCCCAATCTCGCTCAG	20		
VCA0728F	CCGGTTCGTCAAATCTTCAT	20	758	Hypothetical protein
VCA0728R	TAAAGCGCTCTCAGGTGGTT	20		
VCA0729F	CCAGCATCCACAGAAACCTT	20	462	Hypothetical protein
VCA0729R	TGTGTCTGTCCATTGCCACT	20		
VCA0730F	CACCTTCCAGCTCTTGTTCC	20	486	Hypothetical protein
VCA0730R	ATACCTACGCCTTGCACCAC	20		

et al., 2004). However, PCR identification of other neighbouring genes (*rstA*, $gIII^{CTX}$ and *zot*) indicated the presence of an intact core region of the CTX prophage genome. *rstR* is a regulatory gene and present in the RS2 part of the CTX prophage. This gene has four variants: $rstR^{classical}$, $rstR^{El\ Tor}$, $rstR^{Calcutta}$ and $rstR^{environmental}$, and our previous studies (Ansaruzzaman *et al.*, 2004; Nair *et al.*, 2002; Nusrin *et al.*, 2004) have shown that either a single *rstR* variant or an assortment of *rstR* variants is present in all the strains tested. Kimsey *et al.* (1998) first reported the presence of different types of *rstR* in a single *V. cholerae* strain, but the implication of this assortment is not yet known. Faruque *et al.* (2002) have recently shown that RS1 is a self-transducing phage, and that the *rstC* gene acts as an antirepressor in the phage replication process (Davis & Waldor, 2003). This gene is unique to the strains of the El Tor biotype and is absent in classical strains. Thus, we checked all the strains for the *rstC* gene and found that 10 strains, including Mozambique strains, lacked the *rstC* gene (Table 1). In other words, the absence of the *rstC* gene classified these strains as classical type, which is contrary to the earlier findings with the *tcpA* gene, but matches the *rstR* result obtained in our previous studies (Ansaruzzaman *et al.*, 2004; Nusrin *et al.*, 2004). Notably, all the *rstC*-negative strains were also negative for the TLC (Table 1), and require further examination to understand the relationship.

Recent studies have reported that *rtxC*, which encodes the activator protein, is absent from strains of classical biotype and present in the El Tor biotype only (Dziejman *et al.*, 2002; Lin *et al.*, 1999; O'Shea *et al.*, 2004). The presence of the *rtxC* gene grouped all the strains as El Tor biotype. The VSP-I gene cluster encompasses a 16 kb region from VC0175 to VC0185, and most of the genes encode hypothetical or

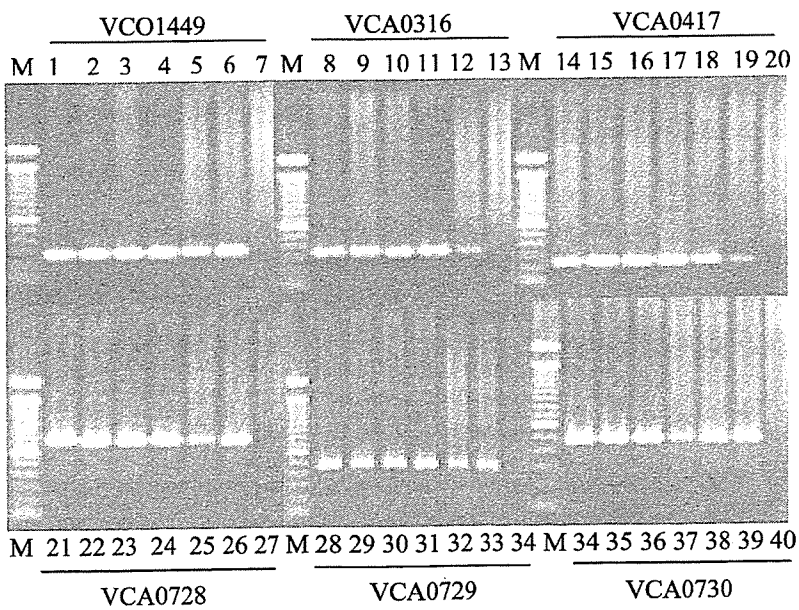

Fig. 1. Gel image showing amplified genes indicated by the annotation numbers given in Table 2. Lane M, molecular size marker (100 bp ladder); lanes 1–5, 8–11, 14–18, 21–25, 28–32 and 34–38 represent Matlab type strains MJ1236 (MT-I), MJ1485 (MT-I), MG116226 (MT-II), MG116025 (MT-III) and MG116926 (MT-III), respectively; lanes 6–7, 12–13, 19–20, 26–27, 33–34 and 39–40 represent *V. cholerae* El Tor N16961 and the classical 569B reference strain.

conserved proteins with no known function. On the other hand, the VSP-II region is a ~27 kb region that encompasses VC0490 to VC0516 (O'Shea *et al.*, 2004). As these two clusters are unique to the El Tor strains of the seventh pandemic, finally we checked for the presence of VSP-I and -II in the genome of these strains. All strains examined were positive for VSP-I and -II, pointing to the seventh-pandemic El Tor ancestry of these strains. The presence of VSP-I and -II also indicated that these strains have the potential to initiate pandemic spread, as these two regions are thought to be associated with the pandemicity of the El Tor biotype. Dziejman *et al.* (2002) also identified six genetic loci that are unique to strains of the El Tor biotype but absent from the classical biotype (Fig. 1). All these loci encode either hypothetical proteins or a putative acetyl transferase. All the six loci were present in all strains tested, except the classical reference strain, which further underscores the El Tor lineage of these strains.

On the basis of DNA and protein sequencing, heterogeneity within the B subunit was first reported in the early 1990s (Brickman *et al.*, 1990; Kaper *et al.*, 1995), and since then *ctxB* typing has been used as a tool for differentiating *V. cholerae* strains. To date, three *ctxB* genotypes of *V. cholerae* O1 strains of both biotypes and serotypes have been identified globally (Mekalanos *et al.*, 1993; Olsvik *et al.*, 1993). Based on the amino acid residue substitution at the three positions 39, 46 and 68, all classical and El Tor strains from the Gulf Coast of the USA are categorized as *ctxB* of genotype 1, El Tor strains associated with the Australian environmental reservoir are genotype 2, and El Tor strains of the seventh pandemic and the recent Latin American epidemic are classified as *ctxB* genotype 3. In this study, all except two strains examined possessed the classical type of *ctxB* DNA sequence or genotype 1, which is in contrast to the results obtained by PCR from different virulence-associated genetic regions. Notably, the PFGE results from our previous study (Safa *et al.*, 2005) that clustered reference strains (MT-I, MT-II and MT-III) of Matlab variants with the El Tor biotype also disagree with the *ctxB* typing result.

The overall analysis showed that in all these Matlab variants most of the genetic traits tested are El Tor-like, indicating that these have an El Tor genome backbone. In contrast, the classical biotype attributes in these strains are mainly confined to the CTX prophage region, which is typically the classical CTX prophage. Lee *et al.* (2006) have recently shown that the Mozambique strains of El Tor biotype carry a tandem array of the classical prophages. Furthermore, in 1961, with the beginning of the seventh pandemic, the classical strains were gradually replaced by the El Tor biotype, and in Bangladesh the replacement started from 1968 and ended by 1973. However, the classical biotype reappeared in 1982 (Samadi *et al.*, 1983) in Bangladesh and caused disease until 1993. Interestingly, the Matlab variants were isolated during a period when the classical biotype was disappearing from Bangladesh for the second time. The hybrid make-up of these strains thus appears to be built on the El Tor backbone, in which classical biotype attributes might have been acquired through horizontal gene transfer from classical strains that were on the verge of extinction. The similarity of PCR results and identical DNA sequence of the *ctxB* gene of these Matlab variants to those of the strains isolated during a recent outbreak in Mozambique are also key observations of this study which underscore the epidemiological significance of these variants.

ACKNOWLEDGEMENTS

The Japan Health Science Foundation funded this study. ICDDR,B acknowledges with gratitude the commitment of the Japan Health Science Foundation to the Center's research efforts.

REFERENCES

Albert, M. J., Siddique, A. K., Islam, M. S., Faruque, A. S. G., Ansaruzzaman, M., Faruque, S. M. & Sack, R. B. (1993). Large outbreak of clinical cholera due to *Vibrio cholerae* non-O1 in Bangladesh. *Lancet* **341**, 704.

Altschul, S. F., Madden, T. L., Schaffer, A. A., Zhang, J., Zhang, Z., Miller, W. & Lipman, D. J. (1997). Gapped BLAST and PSI-BLAST: a new generation of protein database search programs. *Nucleic Acids Res* **25**, 3389–3402.

Ansaruzzaman, M., Bhuiyan, N. A., Nair, G. B., Sack, D. A., Lucas, M., Deen, J. L., Ampuero, J., Chaignat, C. L. & The Mozambique Cholera Vaccine Demonstration Project Coordination Group (2004). Cholera in Mozambique, variant of *Vibrio cholerae*. *Emerg Infect Dis* **10**, 2057–2059.

Barrett, T. J. & Blake, P. A. (1981). Epidemiological usefulness of changes in hemolytic activity of *Vibrio cholerae* biotype El Tor during the seventh pandemic. *J Clin Microbiol* **13**, 126–129.

Brickman, T. J., Boesman-Finkelstein, M., Finkelstein, R. A. & McIntosh, M. A. (1990). Molecular cloning and nucleotide sequence analysis of cholera toxin genes of the CtxA$^-$ *Vibrio cholerae* strains Texas Star-SR. *Infect Immun* **58**, 4142–4144.

Brown, M. H. & Manning, P. A. (1985). Haemolysin genes of *Vibrio cholerae*: presence of homologous DNA in non-haemolytic O1 and haemolytic non-O1 strains. *FEMS Microbiol Lett* **30**, 197–201.

Chow, K. H., Ng, T. K., Yuen, K. Y. & Yam, W. C. (2001). Detection of RTX toxin gene in *Vibrio cholerae* by PCR. *J Clin Microbiol* **39**, 2594–2597.

Davis, B. M. & Waldor, M. K. (2003). Filamentous phages linked to virulence of *Vibrio cholerae*. *Curr Opin Microbiol* **6**, 35–42.

Davis, M. B., Moyer, K. E., Boyd, E. F. & Waldor, M. K. (2000). CTX prophages in classical biotype *Vibrio cholerae*: functional phage genes but dysfunctional phage genomes. *J Bacteriol* **182**, 6992–6998.

DiRita, V. J., Neely, M., Taylor, R. K. & Bruss, P. M. (1996). Differential expression of ToxR regulon in classical and El Tor biotypes of *Vibrio cholerae* is due to biotype-specific control over ToxT expression. *Proc Natl Acad Sci U S A* **93**, 7991–7995.

Dziejman, M., Balon, E., Boyd, D., Fraser, C. M., Heidelberg, J. F. & Mekalanos, J. J. (2002). Comparative genomic analysis of *Vibrio cholerae*: genes that correlate with cholera endemic and pandemic disease. *Proc Natl Acad Sci U S A* **99**, 1556–1561.

Faruque, S. M., Albert, M. J. & Mekalanos, J. J. (1998). Epidemiology, genetics, and ecology of toxigenic *Vibrio cholerae*. *Microbiol Mol Biol Rev* **62**, 1301–1314.

Faruque, S. M., Asadulghani Kamruzzaman, M., Nandi, R. K., Ghosh, A. N., Nair, G. B., Mekalanos, J. J. & Sack, D. A. (2002). RS1 element of *Vibrio cholerae* can propagate horizontally as a filamentous phage exploiting the morphogenesis genes of CTXΦ. *Infect Immun* **70**, 163–170.

Heidelberg, J. F., Eisen, J. A., Nelson, W. C. & 29 other authors (2000). DNA sequence of both chromosomes of the cholera pathogen *Vibrio cholerae*. *Nature* **406**, 477–483.

Heilpern, A. J. & Waldor, M. K. (2003). $pIII^{CTX}$, a predicted CTXΦ minor coat protein, can expand the host range of coliphage fd to include *Vibrio cholerae*. *J Bacteriol* **185**, 1037–1044.

Herrington, D. A., Hall, R. H., Losonsky, G., Mekalanos, J. J., Taylor, R. K. & Levine, M. M. (1988). Toxin, toxin-coregulated pili, and the *toxR* regulon are essential for *Vibrio cholerae* pathogenesis in humans. *J Exp Med* **168**, 1487–1492.

Jonson, G., Holmgren, J. & Svennerholm, A. M. (1991). Identification of a mannose-binding pilus on *Vibrio cholerae* El Tor. *Microb Pathog* **11**, 433–441.

Kaper, J. B., Bradford, H. B., Roberts, N. C. & Falkow, S. (1982). Molecular epidemiology of *Vibrio cholerae* in the U. S. Gulf Coast. *J Clin Microbiol* **16**, 129–134.

Kaper, J. B., Morris, J. G., Jr & Levine, M. M. (1995). Cholera. *Clin Microbiol Rev* **8**, 48–86.

Karalois, D. K. S., Lan, R. & Reeves, P. R. (1995). The sixth and seventh cholera pandemics are due to independent clones separately derived from environmental, nontoxigenic, non-O1 *Vibrio cholerae*. *J Bacteriol* **177**, 3191–3198.

Kimsey, H. H., Nair, G. B., Ghosh, A. & Waldor, M. K. (1998). Diverse CTXΦ and evolution of new pathogenic *Vibrio cholerae*. *Lancet* **352**, 457–458.

Kovach, M. E., Shaffer, M. D. & Peterson, K. M. (1996). A putative integrase gene defines the distal end of a large cluster of ToxR-regulated colonization genes in *Vibrio cholerae*. *Microbiology* **142**, 2165–2174.

Lee, J. H., Han, K. H., Choi, S. Y. & 11 other authors (2006). Multilocus sequence typing (MLST) analysis of *Vibrio cholerae* O1 El Tor isolates from Mozambique that harbour the classical CTX prophage. *J Med Microbiol* **55**, 165–170.

Lin, W., Fullner, K. J., Clayton, R., Sexton, J. A., Rogers, M. B., Calia, K. E., Calderwood, S. B., Fraser, C. & Mekalanos, J. J. (1999). Identification of a *Vibrio cholerae* RTX toxin gene cluster that is tightly linked to the cholera toxin prophage. *Proc Natl Acad Sci U S A* **96**, 1071–1076.

Mazel, D., Dychinco, B., Webb, V. A. & Davies, J. (1998). A distinctive class of integron in the *Vibrio cholerae* genome. *Science* **280**, 605–608.

Mekalanos, J. J., Swartz, D. J., Person, G. D. N., Harford, N., Groyne, F. & deWilde, M. (1993). Cholera toxin genes: nucleotide sequence, deletion analysis and vaccine development. *Nature* **306**, 551–557.

Mitra, S. N., Mukhopadhay, R., Ghosh, A. N. & Ghosh, R. K. (2000). Conversion of *Vibrio* El Tor MAK757 to classical biotype: role of phage PS166. *Virology* **273**, 36–43.

Nair, G. B., Faruque, S. M., Bhuiyan, N. A., Kamruzzaman, M., Siddique, A. K. & Sack, D. A. (2002). New variants of *Vibrio cholerae* O1 biotype El Tor with attributes of the classical biotype from hospitalized patients with acute diarrhea in Bangladesh. *J Clin Microbiol* **40**, 3296–3299.

Nusrin, S., Khan, G. Y., Bhuiyan, N. A. & 9 other authors (2004). Diverse CTX phages among toxigenic *Vibrio cholerae* O1 and O139 strains isolated between 1994 and 2002 in an area where cholera is endemic in Bangladesh. *J Clin Microbiol* **42**, 5854–5856.

Olsvik, Ø., Wahlberg, J., Petterson, B., Uhlen, M., Popovic, T., Wachsmuth, I. K. & Fields, P. I. (1993). Use of automated sequencing of polymerase chain reaction-generated amplicons to identify three types of cholera toxin subunit B in *Vibrio cholerae* O1 strains. *J Clin Microbiol* **31**, 22–25.

O'Shea, A. Y., Reen, J. F., Quirke, A. M. & Boyd, E. F. (2004). Evolutionary genetic analysis of the emergence of epidemic *Vibrio cholerae* isolates on the basis of comparative nucleotide sequence analysis and multilocus virulence gene profiles. *J Clin Microbiol* **42**, 4657–4671.

Recchia, G. D. & Hall, M. R. (1997). Origins of the mobile gene cassettes found in integrons. *Trends Microbiol* **5**, 389–394.

Rivera, I. N., Chun, J., Huq, A., Sack, R. B. & Colwell, R. R. (2001). Genotypes associated with virulence in environmental isolates of *Vibrio cholerae*. *Appl Environ Microbiol* **67**, 2421–2429.

Rubin, E. J., Lin, W., Mekalanos, J. J. & Waldor, M. K. (1998). Replication and integration of a *Vibrio cholerae* cryptic plasmid linked to the CTX prophage. *Mol Microbiol* **28**, 1247–1254.

Safa, A., Bhuiyan, N. A., Alam, M., Sack, D. A. & Nair, G. B. (2005). Genomic relatedness of the new Matlab variants of *Vibrio cholerae* O1 to the classical and El Tor biotypes as determined by pulsed-field gel electrophoresis. *J Clin Microbiol* **43**, 1401–1404.

Samadi, A. R., Shahid, N., Eusuf, A., Yunus, M., Huq, M. I., Khan, M. U., Rahman, A. S. M. M. & Faruque, A. S. G. (1983). Classical *Vibrio cholerae* biotype displaces El Tor in Bangladesh. *Lancet* **1**, 805–807.

Sambrook, J., Fritsch, E. F. & Maniatis, T. (1989). *Molecular Cloning: a Laboratory Manual*, 2nd edn. Cold Spring Harbor, NY: Cold Spring Harbor Laboratory.

Shimada, T., Nair, G. B., Deb, B. C., Albert, M. J., Sack, R. B. & Takeda, Y. (1993). Outbreak of *Vibrio cholerae* non-O1 in India and Bangladesh. *Lancet* **341**, 1347.

Waldor, M. K., Rubin, E. J., Pearson, G. D. N., Kimsey, H. & Mekalanos, J. J. (1997). Regulation, replication, and integration functions of the *Vibrio cholerae* CTXΦ are encoded by region RS2. *Mol Microbiol* **24**, 917–926.

WHO (1987). *Manual for Laboratory Investigations of Acute Enteric Infections*. Geneva: World Health Organization.

TLR-Dependent Induction of IFN-β Mediates Host Defense against *Trypanosoma cruzi*[1]

Ritsuko Koga,* Shinjiro Hamano,† Hirotaka Kuwata,* Koji Atarashi,* Masahiro Ogawa,* Hajime Hisaeda,† Masahiro Yamamoto,‡ Shizuo Akira,‡ Kunisuke Himeno,† Makoto Matsumoto,* and Kiyoshi Takeda[2]*

Host resistance to the intracellular protozoan parasite *Trypanosoma cruzi* depends on IFN-γ production by T cells and NK cells. However, the involvement of innate immunity in host resistance to *T. cruzi* remains unclear. In the present study, we investigated host defense against *T. cruzi* by focusing on innate immunity. Macrophages and dendritic cells (DCs) from MyD88$^{-/-}$TRIF$^{-/-}$ mice, in which TLR-dependent activation of innate immunity was abolished, were defective in the clearance of *T. cruzi* and showed impaired induction of IFN-β during *T. cruzi* infection. Neutralization of IFN-β in MyD88$^{-/-}$ macrophages led to enhanced *T. cruzi* growth. Cells from MyD88$^{-/-}$IFNAR1$^{-/-}$ mice also showed impaired *T. cruzi* clearance. Furthermore, both MyD88$^{-/-}$TRIF$^{-/-}$ and MyD88$^{-/-}$IFNAR1$^{-/-}$ mice were highly susceptible to in vivo *T. cruzi* infection, highlighting the involvement of innate immune responses in *T. cruzi* infection. We further analyzed the molecular mechanisms for the IFN-β-mediated antitrypanosomal innate immune responses. MyD88$^{-/-}$TRIF$^{-/-}$ and MyD88$^{-/-}$IFNAR1$^{-/-}$ macrophages and DCs exhibited defective induction of the GTPase IFN-inducible p47 (IRG47) after *T. cruzi* infection. RNA interference-mediated reduction of IRG47 expression in MyD88$^{-/-}$ macrophages resulted in increased intracellular growth of *T. cruzi*. These findings suggest that TLR-dependent expression of IFN-β is involved in resistance to *T. cruzi* infection through the induction of IRG47. *The Journal of Immunology*, 2006, 177: 7059–7066.

The parasite *Trypanosoma cruzi* is an intracellular protozoan that causes Chagas' disease, a chronic systemic disorder affecting nearly 20 million people in Central and South America. Host defense against *T. cruzi* depends on a variety of cell populations, including NK, CD4$^+$ T cells, CD8$^+$ T cells, and Ig-producing B cells (1–3). In addition, macrophages and dendritic cells (DCs)[3] produce proinflammatory cytokines, such as IL-12, in response to invasion by *T. cruzi* (4–6). IL-12 induces IFN-γ production by NK, CD4$^+$ T cells, and CD8$^+$ T cells. In turn, IFN-γ induces NO production by macrophages and mediates the killing of *T. cruzi* (7, 8). This cytokine milieu is therefore responsible for host resistance to *T. cruzi* infection in vivo. However, it remains uncertain how innate immune cells, such as macrophages and DCs, mediate *T. cruzi*-induced immune responses during the early phase of infection. In addition, *T. cruzi* infection induces the production of type I IFNs (αβ IFN), which possess antiviral activities (9, 10). However, the nature of the involvement of type I IFNs in response to *T. cruzi* infection remains controversial (11).

A family of TLRs has been identified that recognize specific components of various microorganisms, including bacteria, viruses, fungi, and protozoan parasites (12). Recognition of microbial components by TLRs triggers the activation of innate immunity and the subsequent development of Ag-specific adaptive immunity. TLR-mediated signaling pathways originate from the cytoplasmic Toll/IL-1R (TIR) domains, which are conserved among all family members. A group of TIR domain-containing adaptors (MyD88, Toll/IL-1R domain-containing adaptor protein, TIR domain-containing adaptor-inducing IFN-β (TRIF), and TRIF-related adaptor molecule) have been shown to be integral to these TLR signaling pathways (13). The TLR signaling pathways consist of two cascades: a MyD88-dependent pathway and a TRIF-dependent (MyD88-independent) pathway. The MyD88-dependent pathway mediates all TLR-induced productions of proinflammatory cytokines, including IL-12p40, whereas the TRIF-dependent pathway is indispensable for the induction of type I IFNs through TLR3 and TLR4.

Previous studies have analyzed the involvement of TLR-dependent activation of innate immunity in *T. cruzi* infection. TLR2, TLR4, and TLR9 have been implicated in the recognition of *T. cruzi*-derived components (6, 14–16), whereas mice lacking MyD88 were found to be susceptible to the acute phase of *T. cruzi* infection accompanied by defective proinflammatory cytokine production (17). However, even in MyD88-deficient mice, significant IFN-γ production was still observed, indicating the presence of MyD88-independent immune responses. Thus, the nature of the involvement of innate immunity in *T. cruzi* infection still remains to be precisely characterized.

In the present study, we analyzed the involvement of innate immune cells in *T. cruzi* infection using mice lacking both

*Department of Molecular Genetics, Medical Institute of Bioregulation and †Department of Parasitology, Faculty of Medical Sciences, Kyushu University, Fukuoka, Japan, and ‡Department of Host Defense, Institute for Microbial Diseases, Osaka University, and Exploratory Research for Advanced Technology, Japan Science and Technology Agency, Suita, Japan

Received for publication May 31, 2006. Accepted for publication September 1, 2006.

The costs of publication of this article were defrayed in part by the payment of page charges. This article must therefore be hereby marked *advertisement* in accordance with 18 U.S.C. Section 1734 solely to indicate this fact.

[1] This work was supported by grants from the Special Coordination Funds of the Ministry of Education, Culture, Sports, Science and Technology, as well as the Uehara Memorial Foundation, the Mitsubishi Foundation, the Takeda Science Foundation, the Tokyo Biochemical Research Foundation, the Kowa Life Science Foundation, the Osaka Foundation for Promotion of Clinical Immunology, and the Sankyo Foundation of Life Science.

[2] Address correspondence and reprint requests to Dr. Kiyoshi Takeda, Department of Molecular Genetics, Medical Institute of Bioregulation, Kyushu University, 3-1-1 Maidashi, Higashi-ku, Fukuoka 812-8582, Japan. E-mail address: ktakeda@bioreg.kyushu-u.ac.jp

[3] Abbreviations used in this paper: DC, dendritic cell; TIR, Toll/IL-1R; TRIF, TIR domain-containing adaptor-inducing IFN-β; WT, wild type; siRNA, small interfering RNA; EF-1α, elongation factor-1α.

0022-1767/06/$02.00

MyD88 and TRIF, in which all of the previously described TLR-mediated activation mechanisms of innate immunity are totally abolished.

Materials and Methods

Mice

MyD88$^{-/-}$ and TRIF$^{-/-}$ mice were generated as previously described (18, 19). Type I IFN receptor (IFNAR1)$^{-/-}$ mice were purchased from B & K Universal (20). Each mouse strain was backcrossed to C57BL/6 for at least five generations, and then used to generate double-mutant mice. MyD88$^{-/-}$TRIF$^{-/-}$ mice were generated by crossing MyD88$^{+/-}$ TRIF$^{+/-}$ mice. Littermate wild-type (WT) (MyD88$^{+/+}$TRIF$^{+/+}$), MyD88$^{-/-}$ (MyD88$^{-/-}$TRIF$^{+/+}$), and TRIF$^{-/-}$ (MyD88$^{+/+}$TRIF$^{-/-}$) mice were used for the experiments. MyD88$^{-/-}$IFNAR1$^{-/-}$ mice were generated by crossing MyD88$^{+/-}$IFNAR1$^{+/-}$ mice, and used for the experiments at 8–10 wk of age. All animal experiments were conducted in accordance with the guidelines of the Animal Care and Use Committee of Kyushu University.

Preparation of macrophages and DCs

To isolate peritoneal macrophages, mice were i.p. injected with 2 ml of 4% thioglycolate medium (Sigma-Aldrich), and peritoneal exudate cells were isolated from the peritoneal cavity at 3 days postinjection. The cells were incubated for 2 h and washed three times with HBSS. The remaining adherent cells were used as peritoneal macrophages in experiments. To prepare bone marrow-derived DCs or macrophages, bone marrow cells were prepared from the femur and tibia, passed through a nylon mesh and cultured in RPMI 1640 medium supplemented with 10% FBS, 100 mM 2-ME, and 10 ng/ml GM-CSF (PeproTech) or 30% L cell culture supernatant. After 6 days, the cells were used as DCs or macrophages in experiments.

Parasites and experimental infection

The *T. cruzi* Tulahuén strain was maintained in vivo in IFN-γR$^{-/-}$ mice by passages every other week (21). For in vitro experiments, macrophages or DCs (5×10^4) were infected with 5×10^4 trypomastigotes. After 6 h of infection, the cells were washed twice with PBS to remove the extracellular parasites and cultured in RPMI 1640 supplemented with 10% FBS for the indicated time periods. Trypomastigotes in the culture supernatants were counted microscopically. Alternatively, the cells were pulsed with 1 μCi of [^{3}H]uracil and cultured for 72 h. The cells were then harvested on glass fiber filters and the incorporated uracil was measured using a liquid scintillation counter. The net cpm was calculated by subtracting the background cpm in uninfected cultures from the cpm of the infected cultures. In some experiments, macrophages were infected with *T. cruzi* in the absence or presence of 10 ng/ml of an anti-IFN-β neutralizing Ab (YAMASA) for 6 h, washed and then further cultured with or without the anti-IFN-β Ab.

In other experiments, extracellular parasites were removed by repeated washing after 6h of infection, and the cells were incubated for a further 48 h. Subsequently, the cells were washed, fixed and stained using a Diff-Quik kit (Sysmex). The intracellular parasite numbers in 250 macrophages were counted under a light microscope. Counting was performed in a blinded manner by two independent investigators.

For in vivo experiments, mice were i.p. injected with plasma containing 2×10^3 or 1×10^4 trypomastigotes as indicated. The number of parasites in the blood of each animal was then counted microscopically using 5 μl of blood taken from the tail. Statistical significance was determined using a paired Student's *t* test. Differences were considered to be statistically significant at $p < 0.05$.

Measurement of cytokine production

Peritoneal macrophages or DCs (5×10^4) were infected with 5×10^4 *T. cruzi* for 6 h, extensively washed and cultured for 24 h. The culture supernatants were collected and analyzed for their levels of TNF-α by ELISA (Genzyme Techne) and NO using the Griess reagent (Dojindo Laboratories).

Quantitative real-time RT-PCR

Total RNA was isolated with an RNeasy mini kit (Qiagen), and 2 μg of the RNA was reverse-transcribed using M-MLV reverse transcriptase (Promega) and oligo(dT) primers (Toyobo) after treatment with RQ1 DNase I (Promega). Quantitative real-time PCR was performed in an ABI 7000 (Applied Biosystems) using TaqMan Universal PCR Master Mix (Applied Biosystems). All data were normalized to the corresponding level of elongation factor-1α (EF-1α) expression, and the fold difference relative to the EF-1α level was calculated. The amplification conditions were: 50°C (2 min), 95°C (10 min), and 40 cycles of 95°C (15 s), and 60°C (60 s). Each experiment was performed independently at least three times, and the results of one representative experiment are shown. All primers were purchased from Assay on Demand (Applied Biosystems).

RNA interference

For small interfering RNA (siRNA) experiments, dsRNA duplexes targeting the coding region of the GTPase IFN-inducible p47 (IRG47) (5′-GGUGGAUAGUGACUUAUAUtt-3′) were synthesized by Ambion. Bone marrow cells were cultured in the presence of 30% L cell culture supernatant for 6 days. The differentiated bone marrow macrophages were then harvested by 5 mM EDTA treatment and transfected with 1.5 μg of the siRNA using Nucleofector and a Mouse Macrophage Nucleofector kit (Amaxa Biosystems) according to the manufacturer's instructions. The cells were immediately transferred to culture medium and cultured for 18 h. Next, cells were infected with *T. cruzi* for 48 h, and parasite growth was analyzed. To determine the efficiency of gene silencing, cells were infected with *T. cruzi* for 6 h, and the expression of IRG47 mRNA was analyzed by quantitative real-time RT-PCR.

Results

Increased growth of T. cruzi *in MyD88$^{-/-}$TRIF$^{-/-}$ DCs and macrophages*

To study the direct involvement of innate immunity in *T. cruzi* infection, bone marrow-derived DCs prepared from WT, MyD88$^{-/-}$, TRIF$^{-/-}$, or MyD88$^{-/-}$TRIF$^{-/-}$ mice were infected with *T. cruzi*. After 6 h of *T. cruzi* infection, the cells were extensively washed and changed to fresh medium. After culture periods of 4, 5, and 7 days, the number of trypomastigotes released into the culture supernatants were counted (Fig. 1*A*). The culture supernatant of TRIF$^{-/-}$ DCs contained a similar number of trypomastigotes to that of WT DCs. For MyD88$^{-/-}$ DCs, the number of trypomastigotes increased after 5 and 7 days of infection. Furthermore, for MyD88$^{-/-}$TRIF$^{-/-}$ DCs, the number of trypomastigotes increased considerably. Next, peritoneal macrophages were infected with *T. cruzi* (Fig. 1*B*). The number of trypomastigotes in the culture supernatant of MyD88$^{-/-}$ macrophages was slightly increased compared with those of WT or TRIF$^{-/-}$ cells after 5 and 7 days of infection. For MyD88$^{-/-}$TRIF$^{-/-}$ macrophages, larger numbers of trypomastigotes were observed compared with the other cell genotypes after 7 days of infection. Next, replication of *T. cruzi* within macrophages was assessed based on [^{3}H]uracil incorporation (Fig. 1*C*). Intracellular growth of *T. cruzi* was slightly increased in MyD88$^{-/-}$ macrophages, and markedly increased in MyD88$^{-/-}$TRIF$^{-/-}$ cells compared with WT cells. Bone marrow-derived macrophages were also infected with *T. cruzi* and cultured for 48 h, before the number of intracellular parasites was counted. The number of infected cells did not differ among the genotypes (data not shown). However, infected MyD88$^{-/-}$TRIF$^{-/-}$ macrophages contained an increased number of parasites after 48 h of infection (Fig. 1, *D* and *E*). Thus MyD88$^{-/-}$ DCs and macrophages showed a slight increase in *T. cruzi* growth, whereas MyD88$^{-/-}$TRIF$^{-/-}$ cells showed a marked increase in growth, indicating that MyD88$^{-/-}$TRIF$^{-/-}$ DCs and macrophages were defective in the clearance of *T. cruzi*.

Defective T. cruzi *induction of proinflammatory mediators in MyD88$^{-/-}$ macrophages and DCs*

The killing of parasites by macrophages has been shown to be mediated by TNF-α and NO (22–25). Therefore, we next analyzed the production of TNF-α and NO by *T. cruzi*-infected peritoneal macrophages (Fig. 2). Both WT and TRIF$^{-/-}$ macrophages secreted TNF-α and NO in response to *T. cruzi* infection. In contrast,

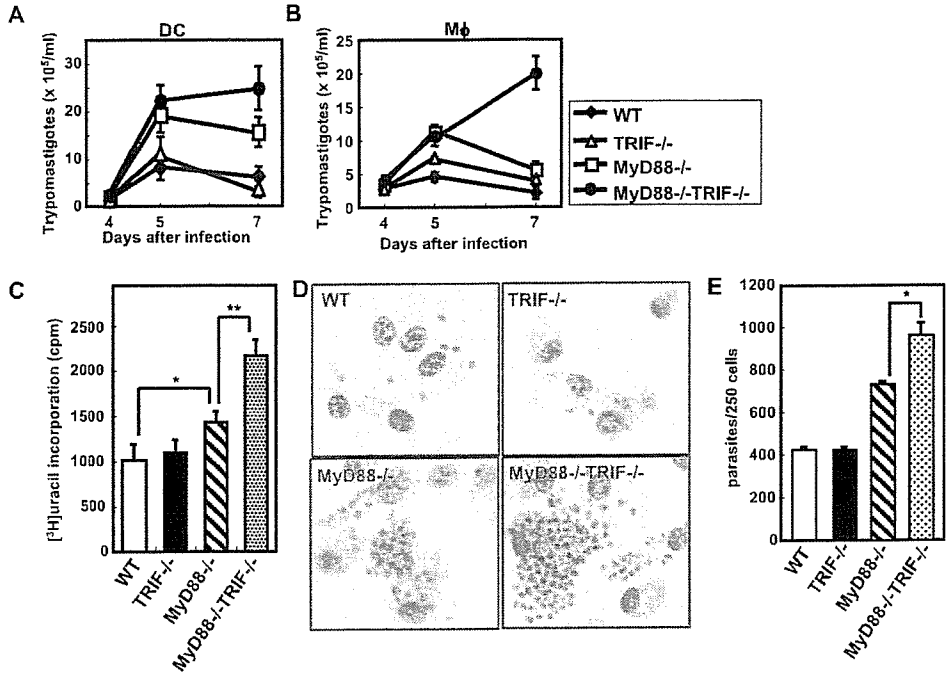

FIGURE 1. Defective *T. cruzi* clearance in MyD88$^{-/-}$TRIF$^{-/-}$ DCs and macrophages. Bone marrow-derived DCs (*A*) or peritoneal macrophages (Mϕ) (*B*) from WT, TRIF$^{-/-}$, MyD88$^{-/-}$, or MyD88$^{-/-}$TRIF$^{-/-}$ mice were seeded onto 96-well plates, and infected with *T. cruzi* for 6 h. The cells were then washed to remove the extracellular parasites and cultured for the indicated periods, before the numbers of trypomastigotes in the culture supernatants were counted. Data are representative of four independent experiments. *C*, Peritoneal macrophages were infected with *T. cruzi*, washed and cultured in the presence of [^{3}H]uracil for 72 h, before the [^{3}H]uracil incorporation was measured. *, $p < 0.01$; **, $p < 0.005$. *D* and *E*, Bone marrow-derived macrophages were infected with *T. cruzi*, washed, and cultured for 48 h. The cells were then fixed, stained, and analyzed by microscopy. Representative stained cells from three independent experiments are shown. Magnification, ×400. The intracellular parasites were counted, and the data represent the mean + SD of the number of parasites per 250 macrophages. *, $p < 0.02$.

secretion of these mediators was severely reduced in both MyD88$^{-/-}$ and MyD88$^{-/-}$TRIF$^{-/-}$ macrophages, and no significant differences were observed between the two genotypes. These findings indicate that *T. cruzi*-induced production of TNF-α and NO was dependent on MyD88, but that the higher susceptibility to *T. cruzi* infection of MyD88$^{-/-}$TRIF$^{-/-}$ macrophages was not due to defective induction of these mediators.

Defective T. cruzi *induction of IFN-inducible genes in MyD88$^{-/-}$TRIF$^{-/-}$ macrophages and DCs*

Next, we tried to identify which genes were selectively less active in *T. cruzi*-infected MyD88$^{-/-}$TRIF$^{-/-}$ DCs. *T. cruzi* infection has been shown to induce IFN-β (9, 10). Therefore, we analyzed *T. cruzi*-induced gene expression focusing on IFN-β and IFN-inducible chemokines as well as proinflammatory cytokines in peritoneal macrophages and DCs from WT, TRIF$^{-/-}$, MyD88$^{-/-}$, and MyD88$^{-/-}$TRIF$^{-/-}$ mice by quantitative real-time RT-PCR. In WT and TRIF$^{-/-}$ macrophages, *T. cruzi* infection led to robust induction of TNF-α and IL-12p40 mRNAs (Fig. 3*A*). In contrast, both MyD88$^{-/-}$ and MyD88$^{-/-}$TRIF$^{-/-}$ macrophages showed defective induction of TNF-α and IL-12p40. Expression of the mRNAs for IFN-β and IFN-inducible genes, such as *Ccl2* (MCP-1), *Ccl5* (RANTES), and *Cxcl10* (IP-10) was induced in *T. cruzi*-infected WT DCs (Fig. 3*B*). In contrast, *T. cruzi*-induced expression of IFN-α4 mRNA was not observed in any of the macrophage and DC genotypes (data not shown). In MyD88$^{-/-}$ DCs, *T. cruzi*-induced expression of *Ccl2*, *Ccl5*, and *Cxcl10* was only slightly reduced. However, DCs from TRIF$^{-/-}$ and MyD88$^{-/-}$TRIF$^{-/-}$ mice showed severely impaired induction of these genes after *T. cruzi* infection. Peritoneal macrophages from each genotype showed similar patterns of *T. cruzi*-induced gene expression (Fig. 3*C*). Thus, MyD88$^{-/-}$ macrophages and DCs showed defective induction of proinflammatory cytokine genes during *T. cruzi* infection, whereas TRIF$^{-/-}$ cells showed defective induction of IFN-β and IFN-inducible genes during the infection. Furthermore, MyD88$^{-/-}$TRIF$^{-/-}$ cells displayed defective expression of all these genes.

IFN-β-mediated inhibition of T. cruzi *growth in MyD88$^{-/-}$ macrophages*

MyD88$^{-/-}$TRIF$^{-/-}$ macrophages and DCs displayed defective clearance of *T. cruzi* with impaired expression of IFN-β and IFN-inducible genes. Therefore, we next addressed whether IFN-β is involved in the resistance to *T. cruzi* infection in MyD88$^{-/-}$ macrophages. Peritoneal macrophages from WT and MyD88$^{-/-}$ mice were infected with *T. cruzi* in the presence of an anti-IFN-β neutralizing Ab, and intracellular growth of *T. cruzi* was measured (Fig. 4). In WT macrophages, *T. cruzi* growth remained unaltered by the addition of the anti-IFN-β Ab. In contrast, anti-IFN-β Ab addition dramatically increased the intracellular growth of *T. cruzi* in MyD88$^{-/-}$ macrophages. These findings indicate the possible involvement of IFN-β in resistance to *T. cruzi* infection in the absence of MyD88.

High-sensitivity to T. cruzi *infection in MyD88$^{-/-}$IFNAR1$^{-/-}$ macrophages*

To further address whether IFN-β is involved in the resistance to *T. cruzi* infection, we generated mice lacking both MyD88 and the IFNAR1 subunit of the $\alpha\beta$ IFN receptor complex (MyD88$^{-/-}$ IFNAR1$^{-/-}$ mice). Bone marrow-derived macrophages were infected with *T. cruzi*, washed, and cultured. After culture periods of 4, 5, and 7 days, the numbers of trypomastigotes in the culture

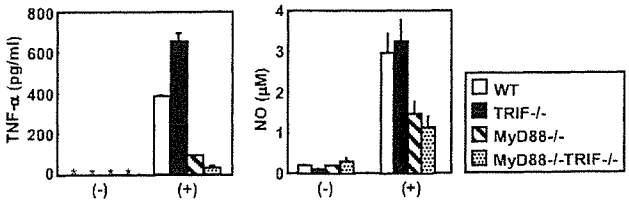

FIGURE 2. Defective production of TNF-α and NO in *T. cruzi*-infected MyD88$^{-/-}$ macrophages. Peritoneal macrophages from WT, TRIF$^{-/-}$, MyD88$^{-/-}$, or MyD88$^{-/-}$TRIF$^{-/-}$ mice were infected with (+) or without (−) *T. cruzi* for 6 h, washed to remove the extracellular parasites, and cultured for 24 h. The levels of TNF-α and NO in the culture supernatants were measured. *, Not detected.

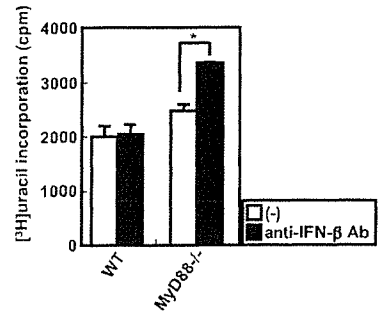

FIGURE 4. Effect of an anti-IFN-β neutralizing Ab on *T. cruzi* growth in macrophages. Peritoneal macrophages from WT or MyD88$^{-/-}$ mice were infected with *T. cruzi* for 6 h in the presence or absence of an anti-IFN-β neutralizing Ab, washed, and cultured in the presence of [^{3}H]uracil for 72 h. The [^{3}H]uracil incorporation was then measured. *, $p < 0.005$.

supernatants were counted (Fig. 5*A*). As mentioned, the culture supernatant of MyD88$^{-/-}$ macrophages contained a larger number of trypomastigotes than that of WT macrophages. In the supernatant of IFNAR1$^{-/-}$ macrophages, a slight increase in the number of trypomastigotes was observed compared with WT cells. Furthermore, the number of trypomastigotes in the culture supernatant of MyD88$^{-/-}$IFNAR1$^{-/-}$ macrophages was considerably increased. Next, intracellular replication of *T. cruzi* was assessed by counting [^{3}H]uracil incorporation (Fig. 5*B*). MyD88$^{-/-}$ and IFNAR1$^{-/-}$ macrophages showed slightly increased growth rates of *T. cruzi*. However, MyD88$^{-/-}$IFNAR1$^{-/-}$ macrophages showed markedly increased growth rates of *T. cruzi* compared with MyD88$^{-/-}$ or IFNAR1$^{-/-}$ cells. Furthermore, at 48 h after the *T. cruzi* infection, increased numbers of parasites were observed in MyD88$^{-/-}$IFNAR1$^{-/-}$ macrophages (Fig. 5, *C* and *D*). Thus, IFNAR1$^{-/-}$ macrophages displayed a slightly increased sensitivity to *T. cruzi* infection, whereas MyD88$^{-/-}$IFNAR1$^{-/-}$ macrophages displayed a higher sensitivity to the infection. These findings suggest that IFN-β is responsible for resistance to *T. cruzi* infection and that this responsibility becomes evident in the absence of MyD88.

High-sensitivity MyD88$^{-/-}$IFNAR1$^{-/-}$ mice to T. cruzi *infection*

Macrophages are the primary site of *T. cruzi* replication, and thus act as the major cell population for controlling the infection in vivo, especially for reticulotropic strains such as the Tulahuén strain used in the present study (21, 26). Therefore, we next addressed whether IFN-β mediates antitrypanosomal responses in vivo. Mice were i.p. infected with *T. cruzi*, and the parasitemia was monitored (Fig. 6*A*). In WT and TRIF$^{-/-}$ mice, the trypomastigote counts in the sera peaked by day 13 of the infection, and subsequently decreased. In IFNAR1$^{-/-}$ mice, serum trypomastigotes were slightly increased compared with WT or TRIF$^{-/-}$ mice, and peaked around 11–13 days of infection. In MyD88$^{-/-}$ mice, the parasite counts were increased at 13 days of infection. In MyD88$^{-/-}$TRIF$^{-/-}$ mice, the serum parasite counts continued to increase, and these mice showed much higher levels of parasitemia by day 15 of infection than levels found in MyD88$^{-/-}$ mice. In MyD88$^{-/-}$IFNAR1$^{-/-}$ mice, the parasite counts increased in a similar manner

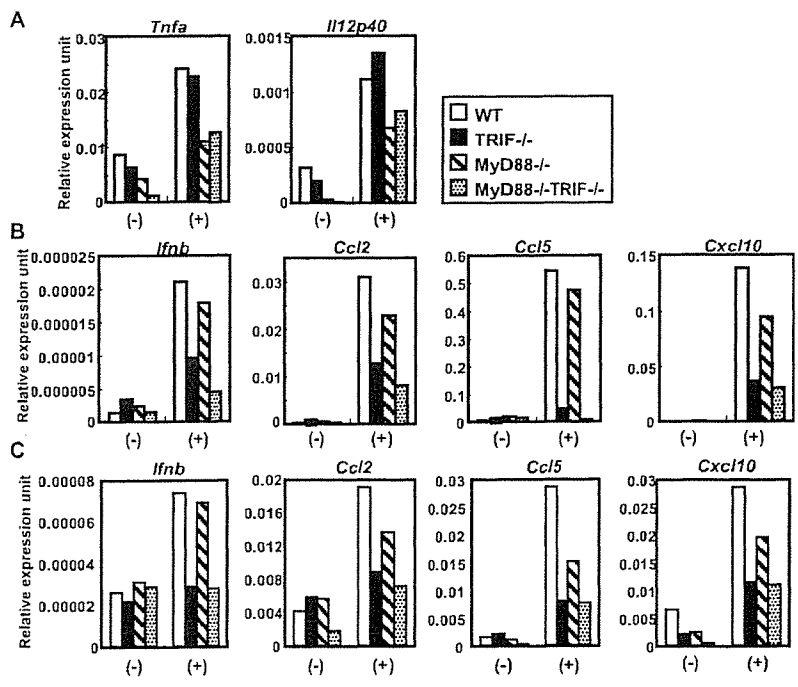

FIGURE 3. *T. cruzi*-induced expression of inflammatory genes in macrophages and DCs. *A*, Peritoneal macrophages from WT, TRIF$^{-/-}$, MyD88$^{-/-}$, or MyD88$^{-/-}$TRIF$^{-/-}$ mice were cultured in the presence (+) or absence (−) of *T. cruzi* for 6 h. Total RNA was then extracted and analyzed for the expressions of *Tnfa* or *Il-12p40* by quantitative real-time RT-PCR. The data are shown as the relative mRNA levels normalized by the corresponding EF-1α mRNA level. Bone marrow-derived DCs (*B*) or peritoneal macrophages (*C*) from WT, TRIF$^{-/-}$, MyD88$^{-/-}$, or MyD88$^{-/-}$TRIF$^{-/-}$ mice were cultured in the presence (+) or absence (−) of *T. cruzi* for 6 h. Total RNA was then extracted and analyzed for the expressions of *Ifnb*, *Ccl2*, *Ccl5*, and *Cxcl10* by quantitative real-time RT-PCR. Data are presented in relative expression units and have been normalized to the corresponding EF-1α mRNA level.